

Heterogeneous & Homogeneous & Bio- & Nano-

CHEMCATCHEM

CATALYSIS

Accepted Article

Title: Xylitol hydrogenolysis over Ru-based catalysts: effect of alkaline promoter and basic oxide modified catalysts

Authors: Maxime Rivière, Noemie Perret, Amandine Cabiac, Damien Delcroix, Catherine Pinel, and Michele Besson

This manuscript has been accepted after peer review and appears as an Accepted Article online prior to editing, proofing, and formal publication of the final Version of Record (VoR). This work is currently citable by using the Digital Object Identifier (DOI) given below. The VoR will be published online in Early View as soon as possible and may be different to this Accepted Article as a result of editing. Readers should obtain the VoR from the journal website shown below when it is published to ensure accuracy of information. The authors are responsible for the content of this Accepted Article.

To be cited as: *ChemCatChem* 10.1002/cctc.201700034

Link to VoR: <http://dx.doi.org/10.1002/cctc.201700034>

WILEY-VCH

www.chemcatchem.org



Xylitol hydrogenolysis over Ru-based catalysts: effect of alkaline promoter and basic oxide modified catalysts

Maxime Rivière,^[a] Noémie Perret,^[a] Amandine Cabiac,^[b] Damien Delcroix,^[b] Catherine Pinel,^[a] Michèle Besson*^[a]

^[a] Univ Lyon, Univ Claude Bernard, CNRS, IRCELYON, UMR5256, Institut de recherches sur la catalyse et l'environnement de Lyon, 2 Avenue Albert Einstein, 69626 Villeurbanne, France

^[b] IFP Energies nouvelles, Rond-Point de l'Echangeur de Solaize, BP 3, 69360 Solaize, France

Abstract

Aqueous phase hydrogenolysis of xylitol into glycols over Ru/C was carried out without and in the presence of a wide range of concentrations of Ca(OH)₂ in order to investigate the reaction pathway. Without base, epimerization and cascade decarbonylation were the predominant reactions with high selectivities to C₅ and C₄ alditols, and light alkanes at full conversion. Glycol production was obtained by addition of Ca(OH)₂ to promote the retro-aldol reaction. It competed with reactions without base and became the main reaction for OH⁻ / xylitol molar ratio $R_{\text{mol}}(\text{OH}/\text{xylitol})$ of 0.13; high selectivities to glycols (56%) and glycerol (16%) were observed. However, lactate (LA) was by-produced up to 27% at high base amount ($R_{\text{mol}}(\text{OH}/\text{xylitol})=0.68$). Bifunctional Ru/metal oxide/C catalysts (metal: Zn, Sn, Mn, Sr, W) were synthesized and were able to cleave C-C bond into glycols without base promoter. 3.1wt.%Ru/MnO(4.5%)/C catalyst was the most active (220 h⁻¹) with reasonable selectivity to glycols (22%) and glycerol (10%) and small production of LA (<1%). Nevertheless, metal oxide leaching of the catalyst was observed likely due to the production of traces of LA.

Keywords

Biomass; base promoter hydrogenolysis; ruthenium catalysts; xylitol

1. Introduction

Due to the growth of worldwide fossil demand for energy and carbon based chemicals along with the environmental problem awareness, the non-edible biomass appears to be a promising alternative resource.^[1–3] Cellulose and hemicelluloses are the most abundant sources of carbon; they can be hydrolyzed to sugar monomers (i.e., glucose, xylose) and then further hydrogenated to the corresponding alditols (i.e., sorbitol, xylitol). In particular, xylitol is listed among the top building blocks as it can generate numerous high added-value derivatives.^[4,5] Hydrogenolysis of polyols yields primarily important glycol derivatives such as ethylene glycol (EG), propylene glycol (PG) and glycerol (GLY). The glycols EG and PG are currently produced in high volume (EG: 25 Mt/y in 2014^[6] and PG: 1 Mt/y in 2013^[7]) from petroleum-based ethylene and propylene via their epoxide intermediates.^[7,8] They are widely used in the manufacture of polyester resins (i.e., PET or PES), in the cosmetic and pharmaceutical industries, and as heat transfer fluids.^[9,10] Their production from renewable biomass could be a complementary process for responding to the increasing demand and to the growing interest of major firms and consumers to introduce biosourced compounds in daily-used products.

The selective catalytic hydrogenolysis of sorbitol^[11–31] and xylitol^[32–37] into glycols has been intensively studied in the last two decades over various supported metal catalysts. Typically, the reaction requires a noble or transition metallic function (Ru, Ni or Cu) for the dehydrogenation/hydrogenation steps and a base to catalyze the C-C cleavage. The reactions are usually carried under harsh conditions, i.e. temperature in the range of 160°C to 230°C and hydrogen pressure in the range of 40 to 120 bar. For instance, a combined EG and PG yield of 54–55% was obtained at nearly full conversion during the hydrogenolysis of xylitol (200°C, 60 bar of H₂) over 90%Cu-SiO₂ catalysts, prepared by deposition-gel method or by deposition-precipitation, and in the presence of Ca(OH)₂.^[34,36] A search through the literature on the hydrogenolysis of alditols revealed that Ru-based catalysts are the most active catalysts.^[14] High conversions of sorbitol were obtained over 3%Ru/carbon nanofiber (86%) and 3%Ru/C (71%), in the presence of CaO base promoter.^[14] Moreover the carrier can impact on the catalytic response. Indeed, Liu *et al.*^[37] studied the effect of the support and reported that carbon-supported Ru catalyst exhibited the highest selectivity to the glycols in the hydrogenolysis of xylitol. When working at 200°C, under 40 bar of H₂ and in the presence of Ca(OH)₂, 56% selectivity towards the glycols was obtained at ca. 25% conversion.^[37] It is challenging to obtain high selectivities to glycols, due to the cascade C-C cleavage by decarbonylation followed by methanation, and the water gas shift reaction generating gaseous by-products and alcohols by C-O cleavage.^[16,28]

Most studies report the addition of a base promoter in aqueous phase in order to facilitate the C-C cleavage via retro-aldol reaction. Ca(OH)₂^[15,35], NaOH^[33] and Ba(OH)₂^[17] are usually employed with a OH⁻/substrate molar ratio in the wide range of 0.07^[25] to 5^[33], but mostly around 0.7.^[21] It is worth noting that the basic additive Ca(OH)₂ has been shown to generate better glycols selectivity results than other hydroxide bases.^[21,27]

The use of large amounts of inorganic homogeneous base requires several separation steps and final neutralization generates high amounts of invaluable salts.^[35] Moreover, alkaline additive favors the formation of lactate as a by-product from glyceraldehyde, at the expense of PG, which limits the selectivity to glycols.^[37] To address these issues, recent studies have reported the use of bifunctional catalysts with basic properties.^[15,18,22–24,26,28,34,35,38] The conversion of sorbitol was studied over a co-precipitated Ni-MgO catalyst without alkaline additive in aqueous phase (200°C, 40 bar of H₂). Around 60% selectivity to glycols, 20% selectivity to glycerol (GLY), and a limited amount of LA were obtained at 68% conversion.^[22] When Ru or Ni-Ru were supported directly on the alkaline promoter calcium hydroxide, the yield to glycols (from sorbitol) was significantly improved, going from 14% over Ru/Al₂O₃ to 28% and 40% over Ru/Ca(OH)₂ and Ni-Ru/Ca(OH)₂, respectively.^[28] However, the catalysts deactivated quickly during the reaction due to solubilization of the support. Ni-Mg-Al catalyst derived from hydrotalcite-like compounds^[23] and co-precipitated Cu/CaO-Al₂O₃^[24] catalysts were shown to be stable for the conversion of sorbitol when working at 200°C / 20 bar and 230°C / 76 bar, respectively; the former one exhibited a selectivity to glycols of 45% and the later one of 61%, at high conversion. 6%Ni deposited on fly ash support^[26] mostly composed of SiO₂, Al₂O₃ and Fe₂O₃, was tested four times for the hydrogenolysis of sorbitol in the absence of base. The catalyst remained stable and high selectivities to glycols (38%) were reported at 200°C and 40% conversion. The group of Liu^[35] impregnated Ni/C with basic oxides (CaO, BaO, CeO₂, La₂O₃, MgO) and tested the catalysts without additional base for xylitol hydrogenolysis at 200°C and under 40 bar H₂. The best activity (20 h⁻¹, normalized per mole of Ni) was obtained over Ni-CeO₂/C with a CeO₂/Ni molar ratio of 1.5 and the best selectivity to glycols (70% at 15% conversion) over Ni-CaO/C with a CaO/Ni molar ratio of 0.66. Nickel did not leach during the reaction, however, the stability of the basic oxide was not addressed.

In this contribution, we considered the modification of a carbon-supported Ru catalyst by addition of five oxides (ZnO, SrO, SnO_x, MnO, WO_x) that present a range of acid-base surface properties. The objective of this work was to investigate the effect of basic oxides on the catalytic activity and products distribution in xylitol hydrogenolysis. ZnO is often used for cellulose or glycerol conversion to EG and PG^[38,39]; SrO is an alkaline oxide in the same group as CaO and MgO; although SnO_x is usually seen as Lewis acid, it has been shown to be an active phase for the retro-aldol reaction of glucose intermediates from cellulose to acetol.^[40] We could not find any literature reporting MnO as active species for C-C cleavage, however it is known to be responsible for the basic character of Ru-MnO_x/C catalyst in the demethoxylation of guaiacol in aqueous media^[41] and for the ring opening reaction of furfuryl alcohol.^[42] For comparison, a bifunctional acidic catalyst was prepared using tungsten oxide. The physicochemical properties of the catalysts (denoted as Ru/MO_x/C) and their catalytic performances were compared. We also investigated the mechanism of xylitol hydrogenolysis over Ru/C catalysis with and without Ca(OH)₂ promoter in order to get further insight on the competitive reactions decarbonylation/epimerization and retro-aldol reaction.

2. Results and Discussion

2.1 Catalyst Characterization

Two Ru/C monometallic catalysts were synthesized by wet impregnation with an aqueous solution of ruthenium(III) nitrosyl nitrate. The bifunctional catalysts, 3wt%Ru/MO_x(y%)/C, where M stands for W, Sn, Sr, Zn, or Mn and y is the wt% of M deposited, were prepared by sequential wet impregnation: metal oxide precursor impregnation, calcination, Ru precursor impregnation, and then reduction. The nominal loading of the second metal M was fixed at 5wt% except for Ru/SrO/C for which it was 3wt%. Table 1 summarizes the Ru and metal oxide loadings, the main textural properties, the metal oxide crystallite sizes, and the basic properties of the catalysts.

Table 1. Metal loadings, total pore volume, BET surface area (S_{BET}), metal oxide crystallite size and total amount of basic sites of the Ru/MO_x/C catalysts.

Catalyst	Metal loading ^[a] [wt%]		M/Ru [wt%/wt%]	Total pore volume [cm ³ .g ⁻¹]	S_{BET} ^[c] [m ² .g ⁻¹]	Crystallite size of MO _x ^[d] [nm]	Total basic sites ^[e] [μmol g ⁻¹]
	Ru	M ^[b]					
Active carbon	-	-	-	0.81	1095	-	n.d
2.9%Ru/C	2.85	-	-	0.84	1087	-	237
7.1%Ru/C	7.09	-	-	0.79	1041	-	n.m.
3.1%Ru/MnO(4.5%)/C	3.13	4.48	1.4	0.88	1120	14	355
2.6%Ru/ZnO(4.1%)/C	2.63	4.10	1.6	0.76	987	18	261
1.8%Ru/SrO(2.1%)/C	1.75	2.14	1.2	0.78	1032	n.d	277
1.6%Ru/SnO _x (5.0%)/C	1.63	5.00	3.1	0.74	933	n.d	156
2.7%Ru/WO _x (5.0%)/C	2.73	5.00	1.8	0.84	971	n.d	85

^[a] Determined by ICP-OES, ^[b] M: W, Sn, Sr, Zn, or Mn, ^[c] relative error: ±5%, ^[d] Debye-Scherrer equation. n.d: not detectable, ^[e] Determined by CO₂-TPD, n.m. not measured.

The final loadings were close to the nominal loadings for Ru/C and Ru/MO_x/C catalysts with M = Mn, Zn and W; the final M/Ru mass ratios were approximately 1.5 for the bimetallic catalysts, as expected. However Ru was not fully deposited for Ru/SrO/C and Ru/SnO_x/C catalysts, with a Ru metal loading around 1.7%.

The N₂ adsorption-desorption isotherms were type IV isotherms (Figure S1)^[43] and exhibited very high adsorption below P/P₀ = 0.1, suggesting that a large proportion of the pore channels are micropores.^[44] Moreover, an increase of adsorbed volume for P/P₀ > 0.8 and hysteresis loops in the desorption branch were observed, indicating the presence of mesopores.^[43-45] The deposition of Ru onto the active carbon support did not change the surface area and pore volume, indicating that the Ru particles did not cause pore blockage (Table 1). The total pore volume of the bifunctional catalysts varied between 0.76 cm³.g⁻¹ and 0.88 cm³.g⁻¹ depending on

the nature of the second metal. Compared to the Ru/C catalysts, the specific surface area is slightly lower (except for Ru/MnO/C), with values in the range 933-1032 m².g⁻¹, suggesting that the textural characteristics of the different catalysts were not strongly affected in spite of the successive treatments, i.e. impregnation, calcination and reduction steps.

The reduction temperature of 450°C was chosen according to literature. Indeed Ru metal particles with small sizes (< 2 nm) were reported for Ru/C^[37] and Ru/ZrO₂ after reduction at 450°C.^[46] Accordingly, the powder X-Ray diffraction (XRD) patterns of the two Ru/C catalysts presented in Figure S2 showed no peaks assigned to metallic Ru (JCPDS 06-0663), suggesting a small crystallite size of Ru⁰ even at high loading (7.1wt% Ru).

The particle size for 2.9wt%Ru/C was characterized by TEM (Figure S3). The sample shows small particles that are well dispersed all over the surface and no agglomerated particles. The mean particle size was estimated to be 1.65 nm from the size distribution. This corresponds to a dispersion of 65%, assuming the particles to be cubic with only five accessible faces.

The XRD patterns associated with the Ru catalysts modified with a basic or acidic oxide are presented in Figure 1. The crystallite mean sizes of the oxides MO_x are included in Table 1.

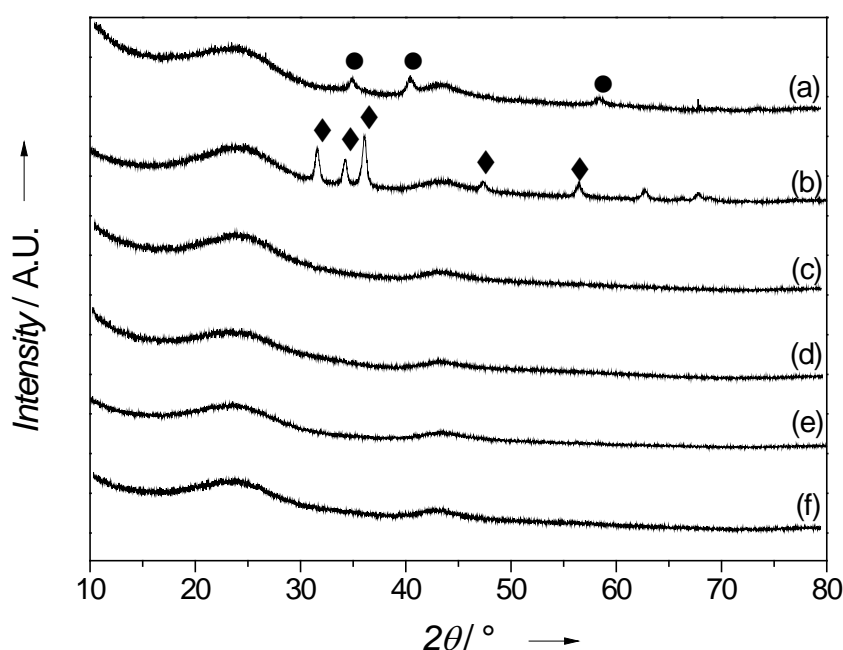


Figure 1. XRD patterns of bifunctional Ru/MO_x/C catalyst with M: a) Mn; b) Zn; c) Sr; d) Sn; e) W, f) active carbon. (●) MnO phase (JCPDS 07-230) and (◆) ZnO phase (JCPDS 36-1451).

After impregnation of the support with the metal oxide precursor, a calcination step was conducted at 200°C under air in order to generate the oxide; the temperature of this heat treatment was limited by the nature of the carrier, i.e. active carbon.

The XRD patterns for reduced Ru/SnO_x/C (Figure 1.d) and Ru/SrO/C (Figure 1.c) did not exhibit diffraction peaks associated with tin or strontium oxide, indicating either a crystallite size below the XRD detection threshold (ca. 3 nm) or amorphous phase properties. In addition, a Ru/SnO_x/C catalyst with a higher Ru (6.6 wt%) and tin oxide (13.5 wt% Sn) loading was synthesized and calcined at two temperatures (200°C under air or 500°C under Ar) however the formation of Ru, RuSn alloy or SnO_x crystallites were still not observed (Figure S4). TEM with EDX analysis of Ru/SnO_x/C showed that Ru and Sn elements were well distributed over the solid. However the presence of chlorine suggests that the precursor was not totally decomposed to SnO_x (Figure S5(a)). Some larger particles, probably SnCl₂, were detected; they were moving under the electron beam and were transformed into SnO₂ (JCPDF 88-0287) (Figure S5(b)). The absence of diffraction peak is surprising since Deng and Liu reported the formation of PtSn alloy (by XRD) in addition to SnO_x species (revealed by XPS), using similar conditions of catalyst synthesis with an Al₂O₃ support and a Sn/Pt atomic ratio exceeding 1.5.^[47] Besides, bimetallic catalysts prepared by incipient wetness impregnation of a 5wt%Ru/C catalyst with an aqueous solution of tin chloride (final catalyst containing 1.6 wt% and 5.5 wt% Sn), followed by heating in air at 80°C for 2 h and reduction in H₂ at 450°C demonstrated multiple phases: Ru, Ru₂Sn₃, Ru₃Sn₇, β-Sn.^[48]

For Ru/ZnO/C (Figure 1.b), diffraction peaks were observed and attributed to ZnO (JCPDS 36-1451) at $2\theta = 31.5^\circ$ (100), 34.2° (002), 36.0° (101), 47.2° (102), and 56.2° (110). The mean crystallite size of ZnO was calculated and was of 18 nm.

The XRD pattern of Ru/WO_x/C (Figure 1.e) did not show any diffraction peak of crystalline WO_x species. Below a monolayer coverage (ca. 5 W/nm²) tungsten oxide is known to be molecularly dispersed on oxide support with high surface area and poorly dispersed on active carbon.^[49] In the latter case, the diffraction peaks of WO₃ are usually not observed below 6.0 wt%.^[49] Raman spectroscopy would be suitable for the discrimination of the molecular structures of supported tungsten oxide species such as isolated surface WO₄ species, polytungstate species, WO₃ crystalline nanoparticles.^[50] However a more detailed characterization of that catalyst was not judged necessary for this study.

The XRD pattern of Ru/MnO_x/C catalyst (Figure 1.a) exhibited peaks at 34.8° , 40.7° , 58.7° attributed to the (111), (200) and (220) cubic planes of MnO phase (JCPDS 07-230); the mean crystallite size was 14 nm. The TEM characterization of the MnO-promoted catalyst shown in Figure S6 confirms the pattern observed by XRD. Small particles of Ru were deposited on both the carbon support and large particles of MnO_x. The oxide phase displayed a particle size around 25 nm.

Ru/MnO/C catalysts with different MnO weight loadings in the range 1.3-19.3 wt% were prepared and characterized. A Ru/MnO_x catalyst was obtained by impregnation of Ru on a synthesized MnO_x support. The physicochemical characteristics of these catalysts are included in Table 2 and the XRD diffraction patterns are presented in Figure 2.

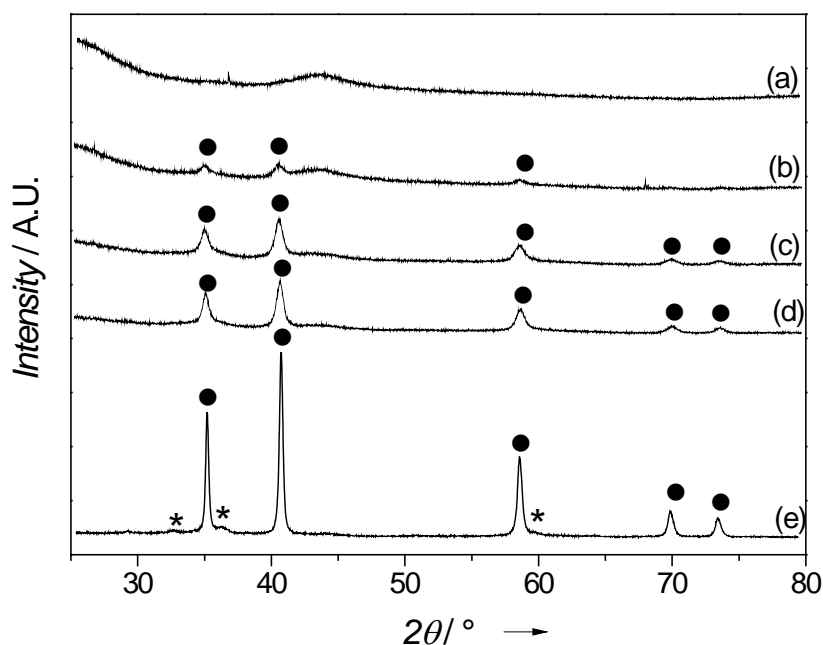


Figure 2. XRD patterns of: a) 3.0%Ru/MnO(1.3%)/C; b) 3.1%Ru/MnO(4.5%)/C; c) 2.9%Ru/MnO(13.4%)/C; d) 3.1%Ru/MnO(19.3%)/C and e) 2.8%Ru/MnO_x. (●) MnO phase (JCPDS 07-230) and (*) Mn₃O₄ phase (JCPDS 24-0734).

Table 2. Ru and Mn loadings, BET surface area (S_{BET}), and mean metal crystallite sizes of Ru/MnO/C and Ru/MnO_x catalysts.

Catalyst	Ru loading ^[a] [wt%]	Mn loading ^[a] [wt%]	Mn/Ru [wt%/wt%]	S_{BET} [m ² .g ⁻¹]	Crystallite size of Mn oxide ^[b] [nm]
3.0%Ru/MnO(1.3%)/C	2.99	1.31	0.4	992	n.d
3.1%Ru/MnO(4.5%)/C	3.13	4.48	1.4	1120	14
2.9%Ru/MnO(13.4%)/C	2.90	13.37	4.6	834	14
3.1%Ru/MnO(19.3%)/C	3.10	19.32	6.2	720	14
2.8%Ru/MnO _x	2.75	-	-	24	n.d

^[a] Determined by ICP-OES, ^[b] Calculated by Debye-Scherrer, n.d: not-detected

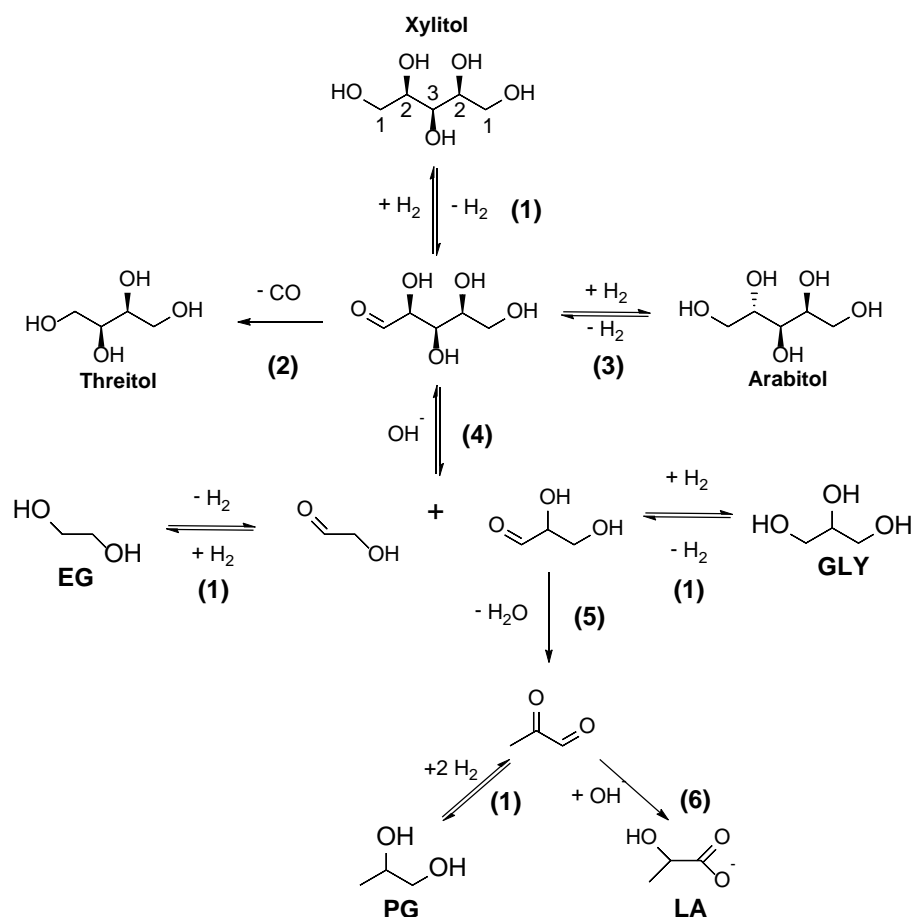
The specific surface area decreased with increasing MnO loading from 1.3% to 19.3%. The manganese species remained as MnO (Figure 2) and the crystallite size of MnO was constant at 14 nm (Table 2). The Ru/MnO_x catalyst prepared on MnO_x carrier (24 m².g⁻¹) demonstrated two phases of MnO_x (Figure 2.e): peaks with the higher intensities were assigned to MnO (JCPDS 07-230), while the smaller peaks at 32.5°, 36.0° and 59.9° were assigned to tetragonal Mn₃O₄ (JCPDS 24-0734). As for Ru/C, no peaks attributed to Ru species were observed, suggesting a high dispersion of Ru on MnO-promoted or MnO_x-supported Ru catalysts, even with low surface area of the latter one.

The basic properties were measured by CO₂-TPD experiments. The CO₂-TPD are comparatively presented in Figure S7, the amounts of CO₂ desorbed are included in Table 1. It is important to note that the detection used was a thermal conductivity detection but without MS. All solids, except the pristine carbon, showed a large desorption peak centered at approximately 425°C. The peak shift to higher temperature observed for Ru/MnO/C and Ru/SnO_x/C indicates that these solids should exhibit relatively stronger basic sites. In addition, a broad signal was shown at 175°C corresponding to basic sites of medium strength for ZnO, SrO and MnO additives. A similar trend for TPD signals was observed in the comparison with literature for Ru/C and Ru-MnO_x/C.^[41] Among the studied materials, the total number of basic sites varied as follows: Ru/MnO/C > Ru/SrO/C > Ru/ZnO/C > Ru/C > Ru/SnO_x/C > Ru/WO_x/C.

To summarize, characterization of the catalysts confirmed the small Ru crystallite size of monometallic Ru/C catalysts even at 7.1 wt% Ru. Based on XRD, the nature of Sr, Sn and W species over active carbon support could not be defined, whereas metal oxide peaks of the second metal were identified for Ru/ZnO/C and Ru/MnO/C. An increase in MnO loadings while keeping Ru loadings constant was associated with a slight decrease in specific surface area of the catalyst, whereas the crystallite size of MnO remained constant. For Ru/MnO_x catalyst, a mixture of two manganese oxide phases, MnO and Mn₃O₄, were observed, on which Ru was well dispersed. The solids presented different basicity properties.

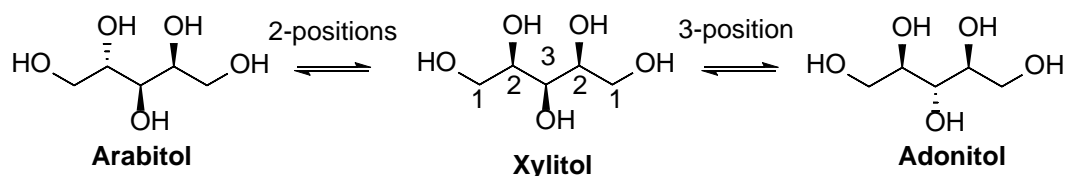
2.2 Hydrogenolysis of xylitol over Ru/C without and in the presence of Ca(OH)₂ base promoter

The hydrogenolysis of polyol to glycols is usually conducted in the presence of a metal catalyst and a basic promoter added to the reaction medium. The simplified and most widely accepted mechanism for the hydrogenolysis of xylitol in the presence of a base is presented in Scheme 1. First, xylitol is dehydrogenated on the 1- position (**1**) to xylose. The aldose can then undergo either a terminal C-C cleavage via decarbonylation reaction (**2**) into threitol, or an enolization and hydrogenation (**3**) into arabitol, an epimer of xylitol, or also a C-C cleavage via retro-aldol reaction (**4**) into glyceraldehyde and glycolaldehyde. These aldehydes can then be hydrogenated respectively into glycerol (GLY) and EG. A dehydration reaction of glyceraldehyde may also occur (**5**) and yields pyruvaldehyde; the latter is either hydrogenated into PG or yields lactate (LA) by Cannizzaro-type disproportionation in basic media (**6**). The retro-aldol reaction cleaves the C-C bond according to the dehydrogenation position of the hydroxyl group. Typically, dehydrogenation of xylitol on the 1-, as (**4**), and 2- positions (not shown) yields C₂ and C₃ products, while dehydrogenation of the 3-position yields C₁ and C₄ products (not shown). Tajvidi *et al.*^[51] proposed also an isomerization of the aldose to ketoses via the so-called Lobry de Bruyn-Alberda van Ekenstein reaction to explain the product distribution they observed over Cu/ZnO/Al₂O₃ catalyst in the absence of a base.^[51]



Scheme 1. Reaction scheme of xylitol hydrogenolysis in the presence of a base, proposed by Sun and Liu.^[37] EG: ethylene glycol, GLY: glycerol, PG: propylene glycol, LA: lactate. Reaction (1) equilibrium dehydrogenation/hydrogenation, (2) decarbonylation, (3) enolization and hydrogenation, (4) retro-aldol reaction, (5) dehydration, and (6) Cannizzaro-type disproportionation.

Through the use of C₃-C₆ alditol stereoisomers, Deutsch *et al.* showed that dehydrogenation of the terminal primary alcohols was favored compared to internal hydroxyl groups, and was followed by decarbonylation.^[16] This was confirmed by H/D exchange of sorbitol in D₂O and the order of dehydrogenation was the following: 1- > 2- >> 3-position.^[52] By kinetic isotopic study on deuterated sorbitol, Jia and Liu showed that the preferential activation step was on the 5-position of sorbitol over Ru/C catalyst in the presence of Ca(OH)₂.^[29] Hence, sorbitol is epimerized more rapidly to mannitol and iditol than to galactitol and allitol. Therefore, from the point of view of kinetics, xylitol would preferentially give arabitol than adonitol (Scheme 2), as reported recently.^[53]



Scheme 2. Possible formation of epimers from xylitol under H_2 pressure, depending on the position of the dehydrogenation step.

We investigated the role of the base promoter by conducting the reaction without $Ca(OH)_2$ additive and in the presence of a wide range of concentrations of the base.

First, no conversion was observed in the blank xylitol hydrogenolysis reactions at $200^\circ C$ under $P_{H_2} = 60$ bar, with or without 0.25 M $Ca(OH)_2$ base, in the absence of a catalyst.

Figure 3 and Figure 4 present the results obtained for xylitol hydrogenolysis as a function of time (a) and as a function of conversion (b), over 2.9% Ru/C in the absence of base (Figure 3) and in the presence of the highest concentration of base investigated, i.e. 0.25 M $Ca(OH)_2$ (Figure 4), respectively.

When no basic additive was introduced, the initial activity was 727 h⁻¹ (normalized to mole of Ru, as described in the experimental section) and xylitol conversion attained 99% after 24 h (Figure 3(a)). Epimers of xylitol (arabitol and adonitol), as well as C_4 polyols (threitol and erythritol) were the main products analyzed in liquid phase within the first 3 h. Afterwards, the concentration of arabitol dropped and those of other products decreased slightly. Compounds with a smaller chain of carbons such as glycerol (GLY), propylene glycol (PG) and also to a lesser degree ethylene glycol (EG), and butanediols (1,2-BDO and 2,3-BDO) were formed. They became the major products in liquid phase at complete xylitol conversion. Traces of methanol were also detected in the aqueous phase. However the low carbon balance in liquid phase reaching only 45% after 24 h indicated that most products were in gas phase. The analysis of the gas phase revealed that light alkanes including CH_4 (83% of carbon in gas phase products), C_2H_6 (9.9%), C_3H_8 (5.2%), C_4H_{10} (1.2%) and C_5H_{12} (0.2%), as well as 0.1% of CO_2 were detected, whereas CO was not present. The amount of carbon measured in the gas phase roughly corresponds to the carbon mass balance defect measured in the aqueous phase. The results are consistent with previous studies which reported that methanation of CO and cleavage of C-O bonds may occur from xylitol^[13,16,28] and xylose^[54] over Ru based catalysts. In addition, these results show that the formation of the gaseous products occurred mainly after 80% xylitol conversion (Figure 3(b)), suggesting that Ru is active for the C-O hydrogenolysis of the products formed from xylitol, i.e. C_4 polyols, GLY, PG and EG, into C_4 - C_1 light alkanes.

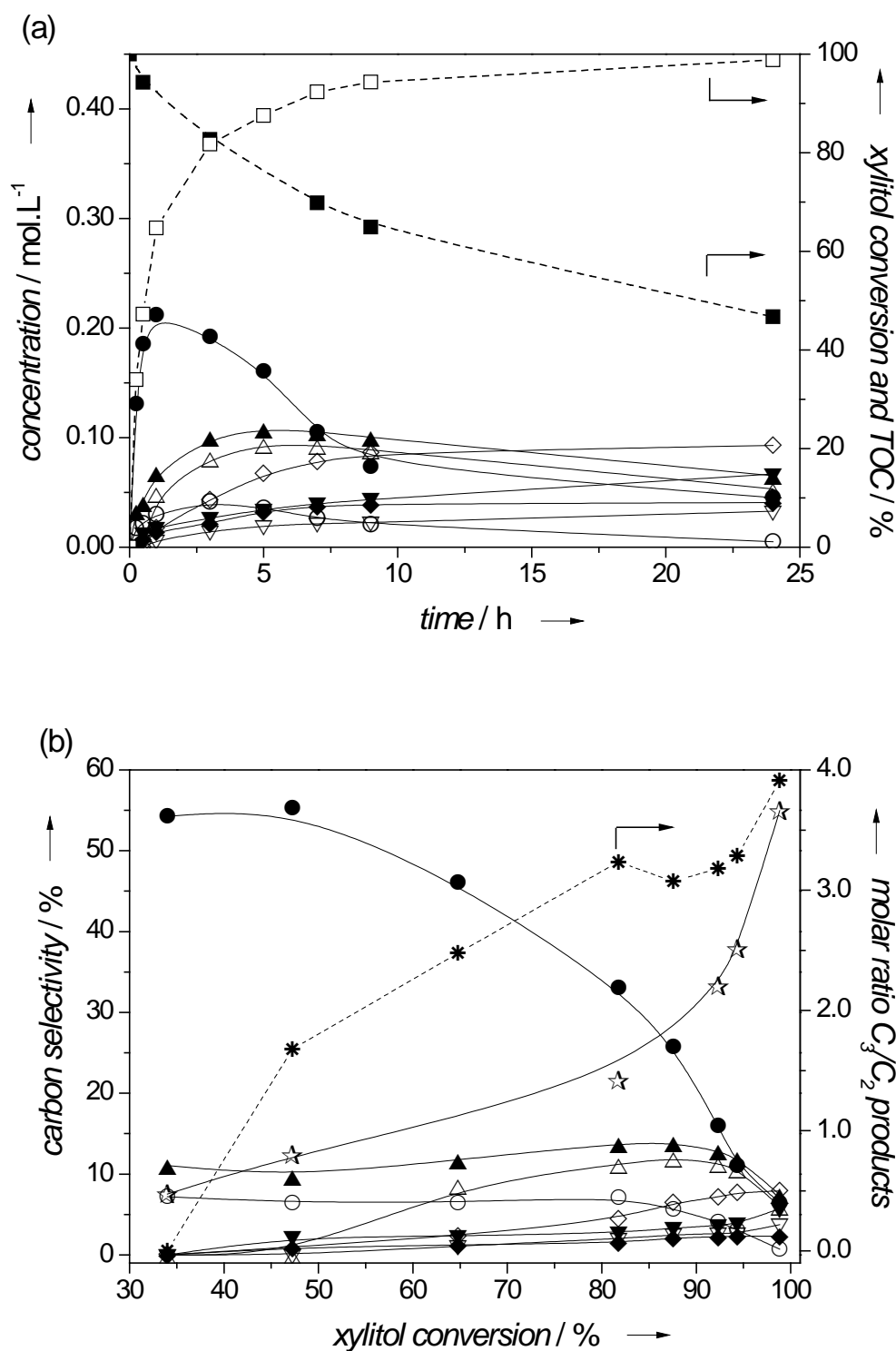
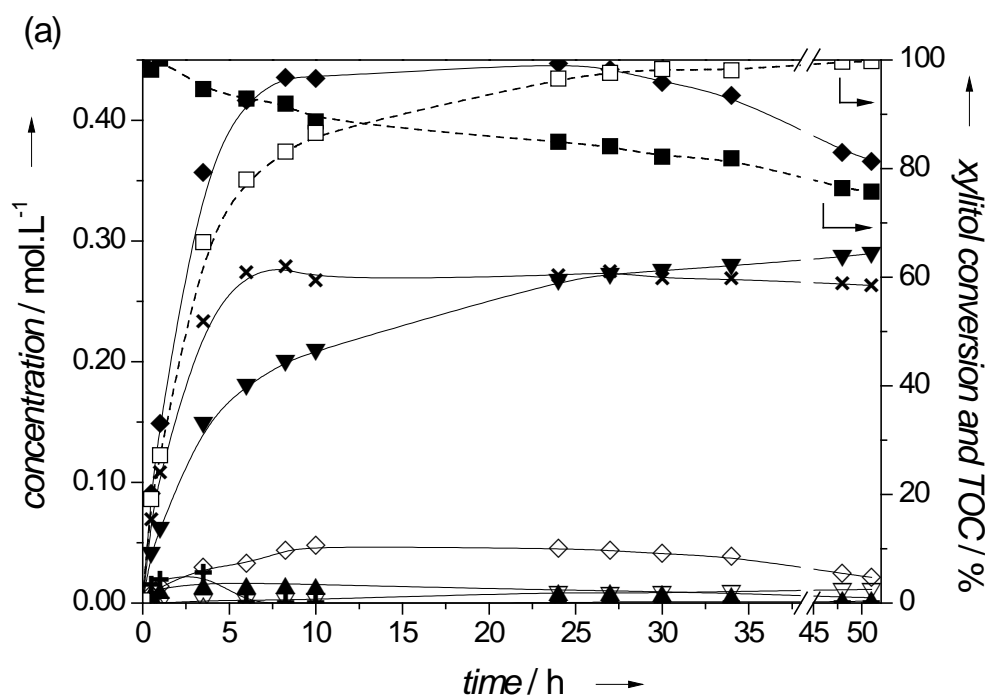


Figure 3. Hydrogenolysis of xylitol over Ru/C without base promoter: (a) xylitol conversion, concentrations profiles, and TOC as a function of time; (b) products distribution as a function of xylitol conversion. (■) TOC measured; (□) Xylitol conversion; (●) Arabitol; (○) Adonitol; (▲) Threitol; (△) Erythritol; (▽) BDO (butanediols); (◇) GLY (glycerol); (▼) PG (propylene glycol); (◆) EG (ethylene glycol); (☆) gas products; (★) C₃/C₂ products molar ratio.

Reaction conditions: xylitol 0.7 mol.L⁻¹ (10 wt%); 135 mL H₂O; 0.5 g 2.9% Ru/C catalyst; 60 bar H₂; 200°C.

The evolution of the product distribution (on a carbon basis, %) towards the different products versus xylitol conversion without base addition is shown in Figure 3(b). The high selectivity to arabitol, up to 55% at 50% xylitol conversion, decreased to 7% at nearly 100% conversion of xylitol. The selectivities to adonitol and threitol remained approximately constant at 12% and 8%, respectively, before they declined for conversion above 90%. The selectivity to erythritol became significant beyond 50% conversion and attained 12%, as for threitol, before decreasing after 90% conversion. Meanwhile, the selectivity to products in the gas phase evolved in inverse proportion to arabitol selectivity, i.e. it increased slowly until 80% conversion and then sharply up to 55% at complete conversion. In parallel, the selectivities to glycols and glycerol were 17% at 99% conversion with a gradual increase of the C₃/C₂ products molar ratio. It should be noted that Ru leaching after reactions was below the detection limit of the ICP-OES analyzer (< 0.2 mg.L⁻¹, < 0.15%). No modification of the XRD pattern of Ru/C catalyst after use was observed suggesting no sintering of the Ru nanoparticles.

The addition of 0.25 M of Ca(OH)₂ base significantly modified the concentration profiles and the products distribution over Ru/C (Figure 4). The reaction proceeded efficiently, however, the activity decreased from 727 h⁻¹ without base to 223 h⁻¹ with 0.25 M Ca(OH)₂. As shown in Figure 4(a), xylitol conversion was nearly complete after 27 h. A similar trend in activity was observed by Sun and Liu^[37] for hydrogenolysis of xylitol over 5wt%Ru/C with the addition of a base. It could be explained by the equilibrium reaction of retro-aldol reaction in the mechanism, which slowed down xylitol conversion. As concerns the pH, the initial value of 12.0 decreased sharply to 7.5 after 10h.



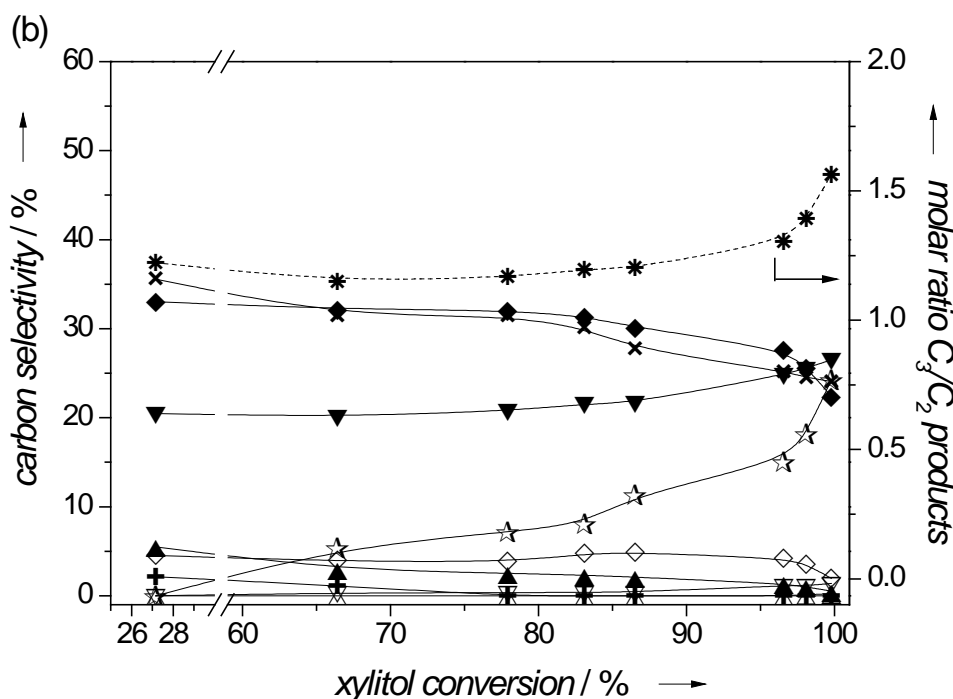


Figure 4. Hydrogenolysis of xylitol over 2.9%Ru/C with 0.25 M of $\text{Ca}(\text{OH})_2$ base promoter: (a) concentrations profiles and xylitol conversion and TOC was a function of time; (b) products distribution as a function of xylitol conversion. (■) TOC measured; (□) Xylitol conversion; (▲) Threitol; (△) Erythritol; (▽) BDO; (◇) GLY; (▼) PG; (◆) EG; (+) FA (formate); (×) LA (lactate); (☆) gas products; (*) C_3/C_2 products molar ratio. Reaction conditions: xylitol $0.7 \text{ mol}\cdot\text{L}^{-1}$ (10 wt%); $135 \text{ mL H}_2\text{O}$; $0.5 \text{ g 2.9\%Ru/C catalyst}$; $2.5 \text{ g Ca}(\text{OH})_2$; 60 bar H_2 ; 200°C .

No epimer of xylitol was generated when adding $\text{Ca}(\text{OH})_2$; on the other hand, traces of C_4 products were observed. The main products were EG, LA and PG. EG and LA reached a plateau at 0.43 M and 0.27 M, respectively, after 8 h. When the reaction time was extended, EG was not stable under the reaction conditions and was gradually consumed after 27 h (i.e. total conversion) whereas LA concentration remained constant. Meanwhile, the PG concentration increased continually up to 52 h, overtaking LA concentration, while GLY concentration remained around 0.05 M up to 24 h and declined afterwards. A small amount of formate (FA) was generated at the beginning of reaction, it reached a maximum of 0.03 M after 3 h and was completely consumed thereafter.

The evolution of selectivities as a function of xylitol conversion in the presence of $\text{Ca}(\text{OH})_2$ is shown in Figure 4(b). Product distribution was essentially unaltered until 80% conversion of xylitol. The C_3/C_2 products molar ratio was approximately constant at 1.25. As the reaction proceeded, the selectivity towards EG, LA, and GLY decreased from 33%, 32% and 4% to 23%, 24% and 1% at full conversion, respectively, whereas the selectivity to PG and products in the gas phase increased sharply from 22% and 10% to 26 and 25%, respectively. Consequently, the C_3/C_2 ratio gradually reached 1.6. A lower production of gaseous products should be noted by comparison with the reaction without base additive (Figure 3(b) and Figure 4(b)); indeed, in the presence of $\text{Ca}(\text{OH})_2$ the selectivity towards gaseous products was 20% at total xylitol conversion compared to 55% in the absence of base. Furthermore, GC analysis of the gas phase indicated that the degradation products consisted mainly of CH_4 (94.6% of carbon

in the gas phase products), C_2H_6 (2.8%) and more CO_2 (1.6%). Presence of C_4 and C_5 alkanes was not detected. After reaction, the solid was recovered by filtration, washed, dried and analyzed by XRD. The phase $CaCO_3$ was detected in addition to the catalyst. During the reaction in basic medium, $Ca(OH)_2$ must react with CO_2 and formed $CaCO_3$.

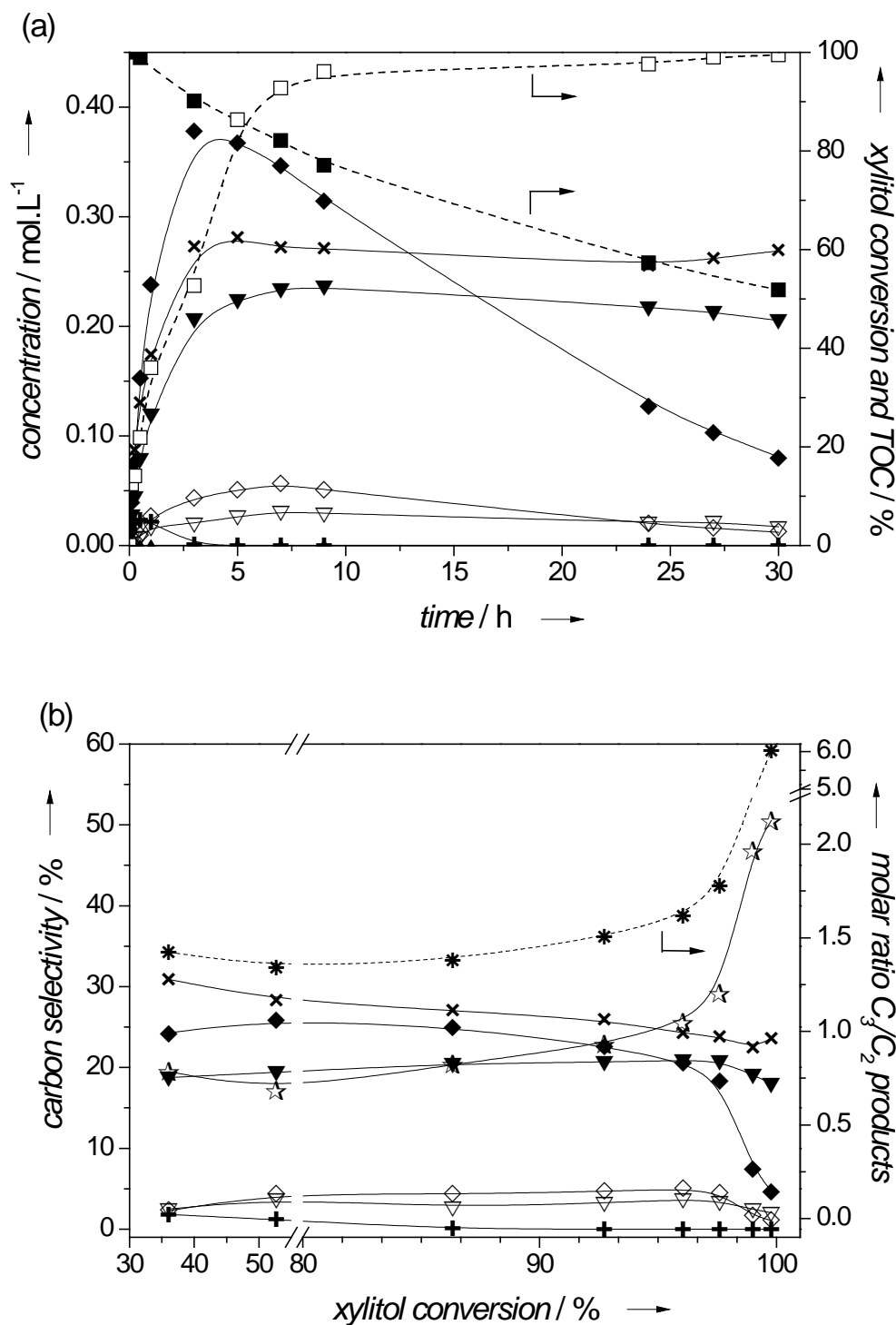


Figure 5. Hydrogenolysis of xylitol over 7.1% Ru/C with addition of 0.25 M Ca(OH)₂ base: (a) xylitol conversion, concentration profiles, and TOC as a function of reaction time; (b) products distribution as a function of xylitol conversion. (■) TOC measured; (□) Xylitol conversion; (▽) BDO; (◇) GLY; (▼) PG; (◆) EG; (⊕) FA; (×) LA; (☆) gas products; (●) C₃/C₂ products molar ratio.

Reaction conditions: xylitol 0.7 mol.L⁻¹ (10 wt%); 135 mL H₂O; 0.5 g 7.1% Ru/C catalyst; 2.5 g Ca(OH)₂; 60 bar H₂; 200°C.

In order to examine the stability of the formed products in the presence of Ru-based catalyst in aqueous solution, the hydrogenolysis of xylitol was conducted over the catalyst containing a

higher Ru loading (7.1 wt%) under the same reaction conditions in the presence of 0.25 M $\text{Ca}(\text{OH})_2$. The results are shown in Figure 5. The activity (202 h^{-1} , normalized to molar Ru) was quite similar to that of 2.9wt% Ru/C (223 h^{-1}) and the reaction was complete after 27 h. However, up to 80% conversion, the selectivities to EG (27%), LA (29%) and PG (20%) over 7.1%Ru/C were slightly lower than the ones observed previously over 2.9%Ru/C (33%, 32%, and 22%, respectively). The C_3/C_2 ratio was 1.45, whereas the selectivity to gaseous products was higher (20% instead of 7% at 80% conversion of xylitol). Beyond 80% conversion, the selectivity to EG dropped, and in parallel the selectivity to gaseous products increased, confirming that EG was converted to gas products over Ru/C.

To further investigate the degradation of EG and identify the products formed, additional reactions were performed using EG as reactant. The reactions were conducted over 2.9%Ru/C with and without $\text{Ca}(\text{OH})_2$ and the results are shown in Figure 6. The catalytic activity observed for the conversion of EG was three times lower in the presence of the base (67 h^{-1}) than without base (194 h^{-1}); a similar ratio was obtained for xylitol reaction. In neutral medium, EG generated methanol (MeOH) as the sole product in liquid phase. MeOH was also observed by Ooms *et al.* during the conversion of aqueous solutions of sugars over Ni- $\text{W}_2\text{C}/\text{AC}$ at 245°C under 60 bar.^[55] In this study, MeOH was then degraded to products which were transferred to the gas phase. Accordingly, TOC analysis of the reaction medium did not detect any carbon left after 7 h, showing that all carbon initially introduced was transferred to the gas phase. In alkaline medium, EG yielded MeOH, small amounts of FA and traces of glycolic acid. Once again, when analyzing the solid residues at the end of the reaction, we could identify CaCO_3 .

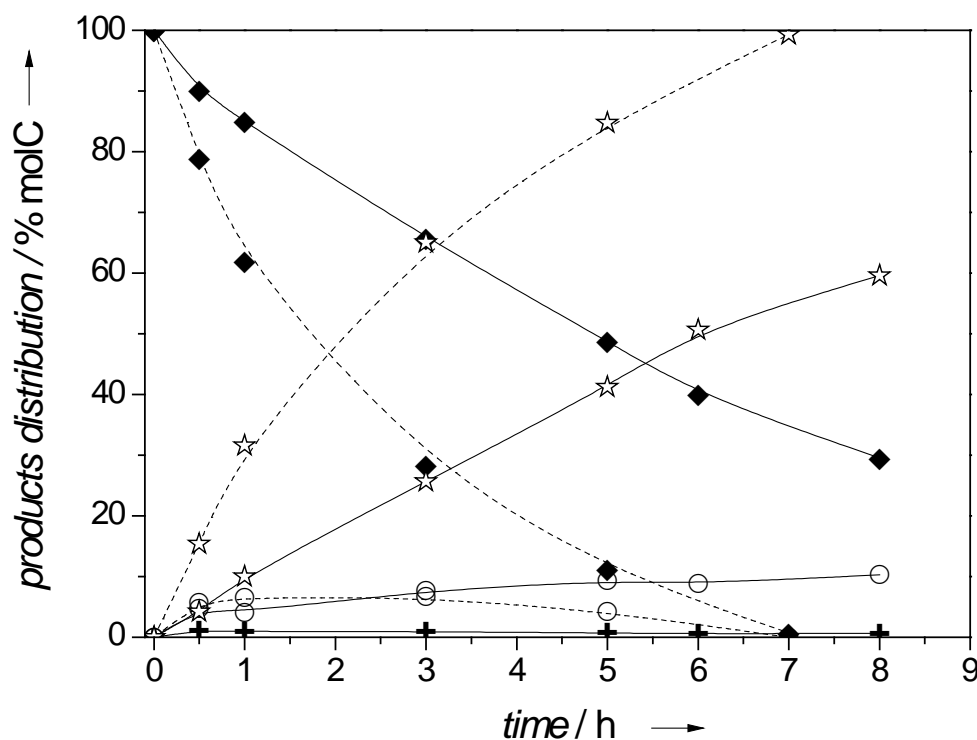
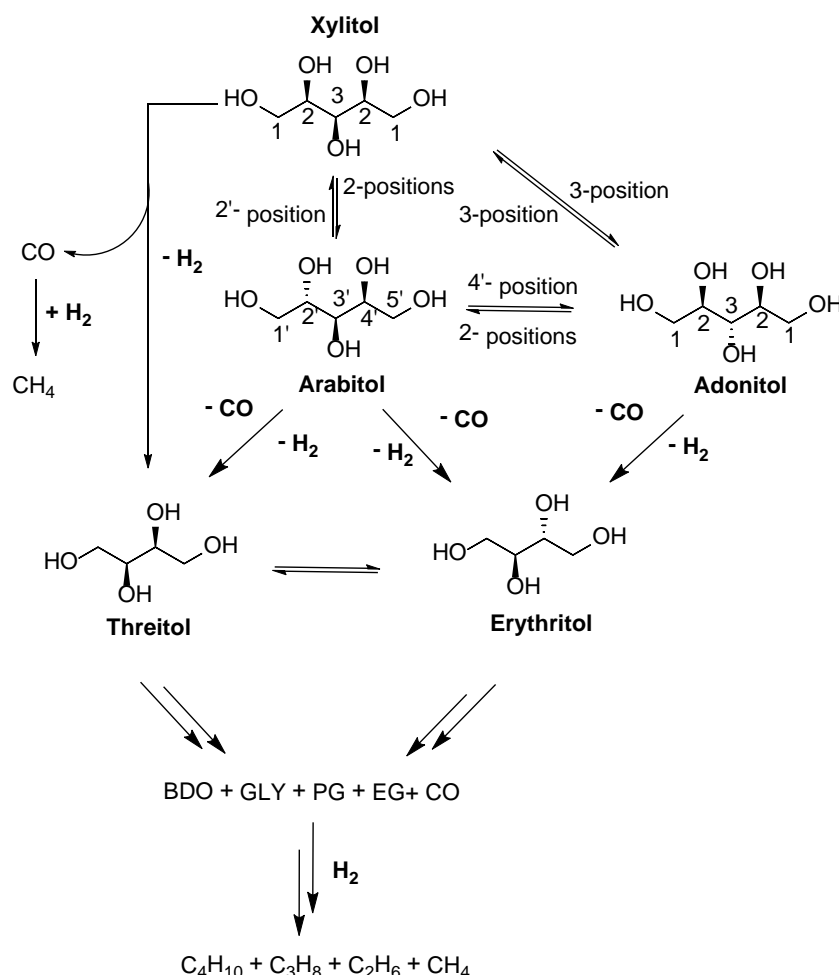


Figure 6. Hydrogenolysis of EG over 2.9%Ru/C in the absence (dotted line) or presence of 0.25 M of Ca(OH)₂ base (full line): (◆) EG; (○) methanol (MeOH) (+) FA; (☆) products in gas phase. Reaction conditions: EG 0.45 mol.L⁻¹ (2.7 wt%); 135 mL H₂O; 0.5 g 2.9%Ru/C catalyst; 0 or 2.5 g Ca(OH)₂; 60 bar H₂; 200°C.

Based on these results, we propose a reaction network under neutral conditions depicted in Scheme 3. First, the results clearly confirm that epimerization and decarbonylation reactions of alditols are predominant reactions in neutral medium over Ru/C.^[16,37,52] Both reactions start by an initial dehydrogenation step of xylitol on metallic sites.

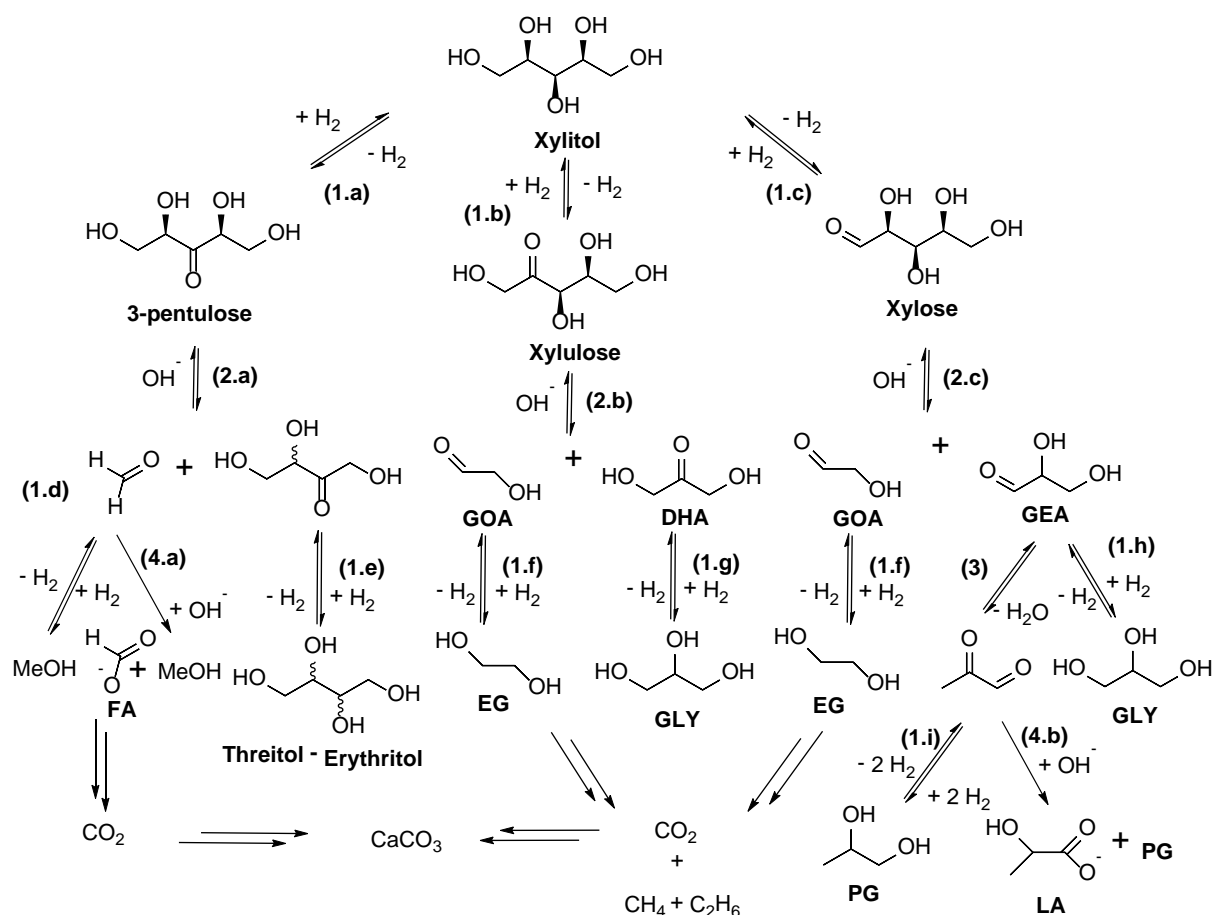


Scheme 3. Reaction network in the absence of a base: possible epimerization and decarbonylation reactions of xylitol. NB: the deoxygenation reaction yielding C₅H₁₂ is not shown due to the very low selectivity observed.

Let us consider the differences in selectivity between the different positions for epimerization. For sorbitol, Hausoul *et al.* showed that the formation of an aldose intermediate by dehydrogenation of the hydroxyl groups located at terminal carbons was easier than the formation of the 2-ketose, and even more than the formation of the 3-ketose, i.e. dehydrogenation of an internal hydroxyl group.^[52] Similar reactions for xylitol dehydrogenation would lead to xylose, xylulose and 3-pentulose, which would then be readily hydrogenated towards xylitol, arabitol and adonitol, respectively. In the present study, the higher selectivity to arabitol compared with the selectivity to adonitol confirms the proposed epimerization mechanism.

Further, the different decarbonylation reactions occurring during xylitol reaction require that the aldose intermediates adsorbed on Ru undergo terminal C-C bond cleavage to yield carbon monoxide and a shorter-chain alditol.^[16] Accordingly, the formation of threitol was observed from the beginning of xylitol reaction, while the formation of erythritol occurred when the selectivity to arabitol started declining, at around 50% conversion (Figure 3(a)). Moreover, we should note that threitol was the major product relative to erythritol, which can be explained as following. Threitol is formed either by xylitol or arabitol decarbonylation; on the other hand, erythritol can be formed by arabitol or adonitol decarbonylation (Scheme 3). Moreover, since the data evidenced that C₄ alditols were produced with different yields, the lower production of adonitol consequently leads to a lower extent of decarbonylation to erythritol. Subsequently, the formation of compounds with shorter carbon chains, such as GLY or EG, results from terminal chain decarbonylation, as proposed by Van der Klis *et al.*^[54] Such reactions result in high production of gaseous products, as observed at the end of reaction. In addition, the formation of BDO is explained by the subsequent dehydration reaction of C₄ alditols (threitol and erythritol) via butanetriols; the latter were observed in very small amounts, making quantification difficult. Similarly, PG was produced by dehydration/hydrogenation of glycerol or dehydrogenation/ decarbonylation of 1,2,3-butanetriol.

In the presence of the base, the retro-aldol reaction is considered as the main reaction in the hydrogenolysis of polyols (Scheme 4).^[27,37,56] A dehydrogenation step is also required before the C-C bond cleavage, which is catalyzed by the hydroxide ions. Starting from xylitol, the dehydrogenation in 1- (step **1.c**) and 2- positions (step **1.b**) produces C₂ and C₃ final products, while dehydrogenation in 3-position (step **1.a**) yields C₁ and C₄ final products.^[51] According to Deutsch *et al.*, the retro-aldol reaction occurring on 3-pentulose is negligible,^[16] combined with the slow dehydrogenation rate in 3- position of xylitol (step **2.a**), this explains the low formation of C₄ and C₁ products in the present study (Figures 4 and 5). However, it was not possible to discriminate the predominance of the retro-aldol reaction in 1-position or 2-position of xylitol (steps **2.b** and **2.c**) since both of them yield C₂ and C₃ products.



Scheme 4. Possible reaction pathways occurring during hydrogenolysis of xylitol over Ru/C catalyst with 0.25 M Ca(OH)₂ base. (1) dehydrogenation/hydrogenation equilibrium, (2) retro-aldol reaction, (3) dehydration, (4) Cannizzaro-type disproportionation. GOA: glycolaldehyde, DHA: dihydroxyacetone, GEA: glyceraldehyde.

Upon prolonged reaction times, the C₃/C₂ molar ratio was higher than 1 owing to the degradation of EG. We propose that EG was dehydrogenated on Ru metal sites and cleaved into two molecules of formaldehyde, as described by Shabaker *et al.*^[57] Ooms *et al.* also observed the conversion of EG into gaseous products (carbon selectivity 86%) and methanol (MeOH) (selectivity 14%) over a Ni-W₂C/AC catalyst in neutral aqueous solution under similar temperature and pressure conditions.^[55] Formate (FA) was formed by Cannizzaro-type disproportionation (**step 4.a**) in basic media while MeOH was formed by hydrogenation of formaldehyde (**step 1.d**) or as a by-product from the **step 4.a**. MeOH and FA were then converted to gaseous products, such as CO₂ (partly converted to CaCO₃) and CH₄ by methanation. The concentration of formate decreased after 5 h and was no more present when the pH became neutral; formaldehyde was then converted to CH₄ and CO₂, as confirmed by the increase of selectivity to gaseous products at 72% xylitol conversion (Figure 5). Furthermore, the C₃/C₂ molar ratio remained constant around 1.25 and then increased at the end of the reaction beyond 72% xylitol conversion. This results in EG degradation, while C₃ products were stable. The use of a catalyst with a higher Ru loading in the presence of 0.25 M Ca(OH)₂ clearly showed EG degradation and the increase of the C₃/C₂ molar ratio after full conversion of xylitol (Figure 5).

2.3 Influence of the amount of $\text{Ca}(\text{OH})_2$ additive over monometallic Ru/C catalyst

We investigated the catalytic performances in term of activities (Table 3) and selectivities (Figure 7) of 2.9%Ru/C for the hydrogenolysis of xylitol in the presence of different concentrations of $\text{Ca}(\text{OH})_2$. The base concentrations were in the range of 3.1 mM (31 mg) to 50 mM (500 mg), i.e. OH^- / xylitol molar ratio $\text{Rmol}(\text{OH}^-/\text{xylitol})$ varied from 0.009 to 0.13. The results were compared to those obtained previously in neutral medium and in the presence of 0.25 M $\text{Ca}(\text{OH})_2$. The selectivities were given at 80% xylitol conversion, before the formation of significant amounts of gaseous products due mainly to the degradation of EG.

Upon introduction of even a very low amount of $\text{Ca}(\text{OH})_2$ (3.1 mM), the catalytic activity significantly decreased from 727 h^{-1} (in the absence of base) to 67 h^{-1} (Table 3). The activity remained approximately at that value upon addition of increasing amounts of the base up to 25 mM. It then increased to 93 h^{-1} with addition of 50 mM of $\text{Ca}(\text{OH})_2$ and to 223 h^{-1} with introduction of 250 mM of $\text{Ca}(\text{OH})_2$. This is in agreement with the literature where it has been reported that the addition of $\text{Ca}(\text{OH})_2$ enhanced the conversion for $\text{Rmol}(\text{OH}^-/\text{sorbitol})$ ratio in the range 0.07-1 during sorbitol hydrogenolysis over Ni/C.^[15,27] The addition of small amounts of base inhibited the reaction, mostly the epimerization reaction to arabitol and adonitol. However, higher amounts increased xylitol conversion by catalyzing the retro-aldol reaction.

Table 3. Activity, C_3/C_2 products molar ratio and carbon balance in the presence of different amounts of $\text{Ca}(\text{OH})_2$ base^[a]

$\text{Ca}(\text{OH})_2$ [mM]	$\text{Rmol}(\text{OH}^-/\text{xylitol})$	Activity [h^{-1}]	C_3/C_2 products molar ratio ^[b]	Carbon balance ^[b] /%	
				TOC	HPLC
None	0.00	727	3.2	83	80
3.1	0.009	67	1.7	79	74
6.7	0.018	65	1.5	83	77
12.2	0.033	67	1.4	85	77
24.4	0.066	75	1.4	86	81
50.0	0.13	93	1.4	93	81
250.0	0.68	223	1.3	91	90

^[a] Reaction conditions: xylitol 10 wt%, 135 mL H_2O , 0.5 g 2.9%Ru/C, 0-2.5 g (0-250 mM $\text{Ca}(\text{OH})_2$), 60 bar H_2 , 200°C.

^[b] at 80% xylitol conversion.

The product distributions at different $\text{Ca}(\text{OH})_2$ loadings are compared in Figure 7. The detailed data are reported in Table S1. The addition of the base using a hydroxyl/xylitol molar ratio of 0.009 was sufficient to initiate C-C cleavage; the yield of glycols (EG + PG) was six times larger than without base. Moreover, the combined selectivity to C_5 alditols (arabitol + adonitol) and C_4 alditols (threitol + erythritol) was divided by two (32% instead of 65%). Thereafter, with increasing addition of $\text{Ca}(\text{OH})_2$, this combined selectivity continued to decrease. The concentrations of C_5 alditols and C_4 products were nearly zero at 50 mM $\text{Ca}(\text{OH})_2$ when glycols reached a maximum of selectivity of 56%. The introduction of higher quantities

of base in the medium ($R_{\text{mol}}(\text{OH}/\text{xylitol}) > 0.13$) induced the production of LA via Cannizzaro-type disproportionation at the detriment of PG and GLY. It may also be noted that increasing the amount of base significantly improved the carbon balance from 79% to 91%.

Without base addition, the quantity of products followed the order $C_5 > C_4 > C_3 > C_2$ which indicates that epimerization and decarbonylation reactions were favored. Moreover, the C_3/C_2 molar ratio (Table 3) was 3.2, indicating that no retro-aldol reaction occurred. Even with a very low amount of base promoter (3.1 mM), the selectivity to C_5 and C_4 products declined and the molar ratio C_3/C_2 decreased to 1.7 as a result of the competition between epimerization and decarbonylation reactions on one hand, and retro-aldol reaction on the other hand. With increasing amounts of $\text{Ca}(\text{OH})_2$ this ratio decreased slowly until 1.3 for 250 mM of $\text{Ca}(\text{OH})_2$. No by-products from decarbonylation and epimerization were then observed. Liu *et al.* studied the hydrogenolysis of xylitol over Cu-SiO₂ and obtained a similar C_3/C_2 molar ratio of 1.2 (at 90% conversion) when working under similar reaction conditions: $\text{Ca}(\text{OH})_2$ base ($R_{\text{mol}}(\text{OH}/\text{xylitol}) = 0.42$), 200°C under 60 bar H₂.^[34]

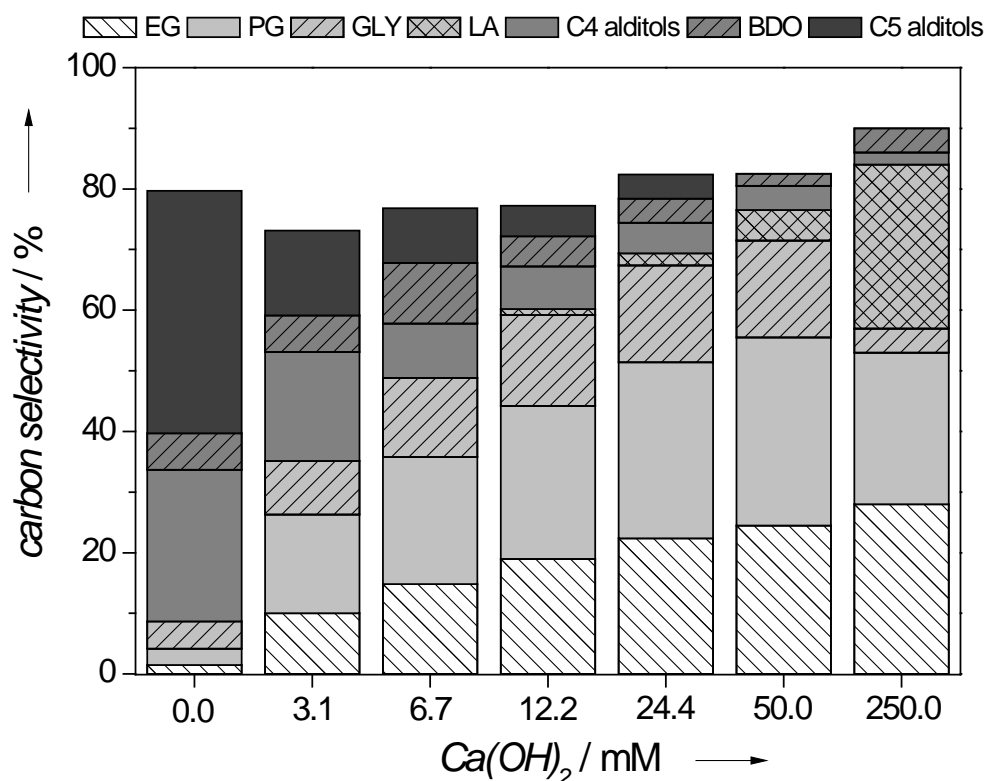


Figure 7. Selectivities in liquid phase at 80% xylitol conversion using different amounts of $\text{Ca}(\text{OH})_2$ promoter. C_5 alditols: arabitol and adonitol; C_4 alditols: threitol and erythritol. Reaction conditions: xylitol 10 wt%, 135 mL H₂O, 0.5 g Ru/C, 0-2.5 g (0-250 mM) $\text{Ca}(\text{OH})_2$ base, 60 bar H₂, 200°C.

Therefore, the use of a high $R_{\text{mol}}(\text{OH}/\text{xylitol})$ promotes the production of C_2 and C_3 products in the hydrogenolysis of xylitol. However, it is also associated with a switch in selectivity towards LA to the detriment of PG. To avoid or to minimize the production of LA, the hydrogenolysis reaction of xylitol was performed on bifunctional catalysts, by modifying the Ru/C catalyst with a basic oxide.

2.4 Promotion of xylitol hydrogenolysis by Ru/metal oxide/C catalyst without Ca(OH)₂ addition

Lactate was produced as a major by-product during xylitol hydrogenolysis under alkaline conditions, obtained when the base promoter Ca(OH)₂ was added to the Ru/C system. According to previous reports, co-deposition of Ni and a solid base (CaO, CeO₂) on active carbon was an efficient way to promote the C-C cleavage of xylitol into glycols with negligible LA production.^[35] In this study, we synthesized catalysts by sequential deposition of a metal oxide and ruthenium and we investigated their catalytic response for the hydrogenolysis of xylitol with and without the addition of the base Ca(OH)₂. The reactions were conducted over 2.9%Ru/C and bifunctional Ru/metal oxide/C catalysts and the results, in term of activity and selectivity (on a carbon basis) to the different products, are given in Table 4. Among the promoters investigated, ZnO,^[38,39] SrO and MnO^[41,42] are considered as basic oxides, WO_x as an acidic oxide and SnO_x as a Lewis acid oxide which can promote the retro-aldol reaction of aqueous glucose solution.^[40]

Without addition of Ca(OH)₂ promoter, with regard to the effect of the metal oxide, the modified catalysts were less active in xylitol hydrogenolysis compared with the Ru/C catalyst. All the oxide-promoted catalysts exhibited an activity at least three times lower than Ru/C: 220 h⁻¹ for Ru/MnO/C, 115 h⁻¹ for Ru/WO_x/C, 84 h⁻¹ for Ru/SrO/C and 13 h⁻¹ for Ru/ZnO/C, compared with 727 h⁻¹ for Ru/C. No clear direct correlation between initial reaction rate (Table 1) and total basicity (Table 4) could be established for the oxide-modified Ru catalysts. The MnO-modified catalyst, which revealed the highest number of total basic sites was the most active; however, the ZnO modified catalyst with significant basicity demonstrated a very low activity. Further characterization of the materials should be performed to identify the active sites. We should note that Ru/SnO_x/C catalyst displayed no catalytic activity towards xylitol conversion. The reason could be due to the presence of SnCl₂ which was not completely decomposed to tin oxides, as shown previously by TEM-EDX analysis. Another reason could be the pre-treatment conditions (reduction of catalyst by H₂ gas at 450°C) that could reduce tin oxide to some metallic tin. Indeed, it has been shown that TPR experiments of Sn catalysts supported on active carbon^[48,58], alumina or zirconia^[59] showed H₂ uptakes in the temperature range of 270°C to 500°C, corresponding to the reduction of Sn⁴⁺ to Sn²⁺ and Sn²⁺ to Sn⁰. This could explain the absence of reaction in the presence of the SnO-promoted catalyst.

As for the products distribution, the selectivity profiles were significantly different and dependent on the nature of the metal oxide. Ru/ZnO/C catalyst significantly favored the C-C cleavage as it exhibited the best selectivity to C₂ and C₃ products (64% combined selectivity) and the lowest selectivity to arabitol (17%). This behavior is in agreement with the relatively high amount of basic sites measured by CO₂-TPD (Table 1). However, the results should be taken with caution. The selectivities to the different products depend strongly on xylitol conversion (Table 4). Or, due to the very low activity of this catalyst, the data are given at 40% xylitol conversion, instead of 80%. Ru/MnO/C and Ru/SrO/C, with significant amount of basic sites (Table 1), were also able to cleave C-C bond to produce glycols with high combined

selectivity to the glycols (23% and 18%, respectively) and to glycerol (8% and 7%, respectively), whereas the selectivity to arabitol was 17% and 20%, respectively. In contrast, Ru/WO_x/C favored the isomerization reaction to arabitol, the decarbonylation to threitol and erythritol, and the cyclization of xylitol to 1,4-anhydroxylitol by a dehydration reaction, known to occur on acidic WO_x sites.^[60]

When the hydrogenolysis reaction was performed in the presence of 0.25 M Ca(OH)₂, the addition of a metal oxide modifier on the solid also diminished the activity of the Ru catalyst but to a lesser extent: from 223 h⁻¹ (Ru/C) to 178 h⁻¹ (Ru/WO_x/C), 90 h⁻¹ (Ru/MnO/C), 88 h⁻¹ (Ru/SrO/C), and 13 h⁻¹ (Ru/ZnO/C). Nevertheless, the influence on the C-C bonds cleavage to C₂ and C₃ products was moderate in the presence of Ca(OH)₂ base, with a global selectivity to the expected glycols remaining approximately 53% for all catalysts. However, Ru/ZnO/C catalyst behaved differently and produced slightly more LA and less glycols than the other catalysts.

In summary, in the absence of base, most of the metal oxide-promoted catalysts investigated in this work were active and more selective than Ru/C for the hydrogenolysis of xylitol to glycols. However, their selectivity to glycols remained lower than in the presence of Ca(OH)₂ base. The interesting point is the formation of only traces of LA under neutral conditions. Unfortunately, an important leaching of the metallic oxide was observed in non-alkaline solutions at the end of the reaction, i.e. 15% of W, 60% of Zn, 71% of Mn, and up to 100% of Sr, making problematic the catalyst recycling.

Table 4. Activity and product distribution in the hydrogenolysis reaction of xylitol over Ru/metal oxide/C catalysts in the absence or presence of Ca(OH)₂ base

Catalyst	Activity [h ⁻¹]	Carbon selectivity [%]					Carbon balance [%]	
		Glycols (EG+PG)	GLY	LA	Arabitol	Others ^[b]	TOC	HP
2.9%Ru/C	727	4	5	0	30	32	83	8
1.6%Ru/SnO_x(5.0%)/C	0	-	-	-	-	-	100	10
2.6%Ru/ZnO(4.1%)/C^[a]	13	56	8	trace	17	5	87	8
1.8%Ru/SrO(2.1%)/C	84	18	7	trace	20	27	81	7
2.7%Ru/WO_x(5.0%)/C	115	12	5	trace	23	40 ^[c]	90	8
3.1%Ru/MnO(4.5%)/C	220	22	10	trace	17	22	84	7
2.9% Ru/C + Ca(OH)₂	223	53	4	27	0	4	91	9
2.6%Ru/ZnO(4.1%)/C + Ca(OH)₂	32	42	0	39	0	0	96	88
1.8%Ru/SrO(2.1%)/C + Ca(OH)₂	88	53	0	32	0	0	95	95
2.7%Ru/WO_x(5.0%)/C + Ca(OH)₂	178	52	4	30	0	0	97	90
3.1%Ru/MnO(4.5%)/C + Ca(OH)₂	90	53	0	34	0	0	90	90

Reaction conditions: 10 wt% xylitol; 200°C; 60 bar H₂; 0.5 g catalyst, Ca(OH)₂ 0 and 0.25 M, at 80% xylitol conversion.

^[a] at 41% xylitol conversion after reaction time 32 h.

^[b] butanediols, threitol, and erythritol

^[c] other products include butanediols, threitol, erythritol, adonitol, and 1,4-anhydroxylitol.

2.5 Further insight in Mn promotion

From the screening of bifunctional catalysts in neutral medium, it appeared that 3.1%Ru/MnO(4.5%)/C exhibited the highest activity and an interesting selectivity to glycols and glycerol, when working in neutral conditions. In order to get greater understanding of the nature of the active Mn species and the effect of MnO on the parameters responsible for C-C bond cleavage and to get a better control and prevent the leaching, the influence of Mn loading of 3%Ru/MnO(y%)/C (y in the range 0-19.3 wt%) was investigated without Ca(OH)₂ additive. The results are displayed in Table 5 and Figure 8.

Table 5. Activity, C₃/C₂ products molar ratio, carbon balance, and Mn leaching of 3%Ru/(y%)MnO/C (y=0-19.3 wt%) as a function of MnO loading, in the hydrogenolysis of xylitol without addition of Ca(OH)₂ base.

Catalyst	Activity [h ⁻¹]	Molar ratio C ₃ /C ₂ products ^[a]	Carbon balance ^[a] [%]		Mn Leaching [%]
			TOC	HPLC	
2.9%Ru/C	727	3.2	83	80	-
3.0%Ru/MnO(1.3%)/C	123	1.9	86	85	63
3.1%Ru/MnO(4.5%)/C	220	1.5	84	71	71
2.9%Ru/MnO(13.4%)/C	344	1.4	83	77	47
3.1%Ru/MnO(19.3%)/C	384	1.5	83	83	68
MnO(4.7%)/C	n.m.	-	100	100	15

^[a] data taken at 80% xylitol conversion. n.m. not measurable.

Reaction conditions: xylitol 10 wt%, 135 mL H₂O, 0.5 g catalyst, 60 bar H₂, 200°C.

MnO(4.7%)/C catalyst displayed a very low conversion (5% conversion after 30 h). Compared to Ru/C, the activity dropped down to 123 h⁻¹ with 1.3% MnO loading on the carbon support. Afterwards, it gradually improved with increasing MnO loading and reached 384 h⁻¹ over 3%Ru-MnO(19.3%)/C. As far as we know, this catalyst is one of the most active catalysts reported in the literature in absence of base for Ru based-catalysts in hydrogenolysis of alditols.^[21] As it was noted previously in free-base conditions for the different additives, the pH value decreased from ca. 7 to ca. 4.3 for Ru/MnO(y%)/C, while it decreased only to 6 in the presence of MnO(4.7%)/C when no reaction occurred.

The selectivities to glycols and glycerol (Figure 8, Table S2) increased also with increasing MnO content, going from 19% to 35% for the glycols (EG+PG) and from 8% to 18% for glycerol. Meanwhile, the selectivity to C₅ alditols dropped from 40% to 10% and the selectivity to C₄ alditols decreased to 10%. These results corroborate the ability of MnO-promoted catalyst to selectively cleave the C-C bonds. Furthermore, MnO/C catalyst without Ru demonstrated no activity, suggesting, as expected, that MnO has no role on the initial dehydrogenation reaction. Notably, only traces of LA were measured, whatever the Mn loading. The percentage of Ru leaching at the end of reaction was less than 0.15% for all reactions, whereas the leaching of

Mn was in the range 47 to 75% independently of the amount of MnO introduced, except for MnO(4.7%)/C where only 15% of Mn leaching was observed.

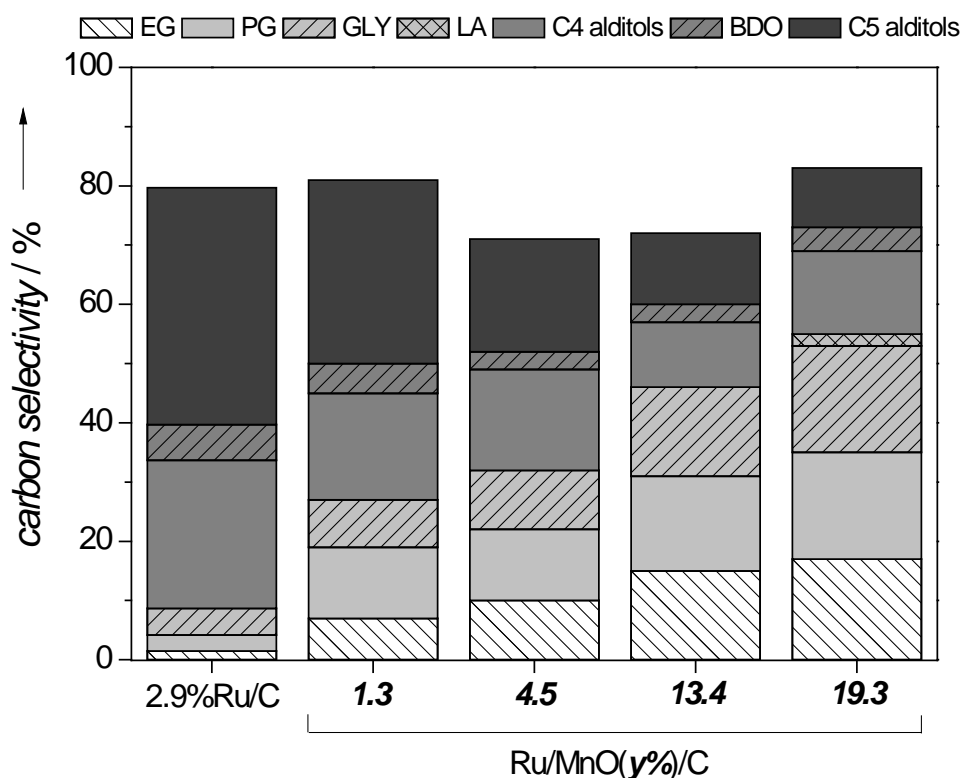


Figure 8. Selectivities to products over 3%Ru/ MnO (y%)/C ($y=0-19.3$ wt %) without addition of $\text{Ca}(\text{OH})_2$ base. C₅ alditols (arabitol+adonitol) and C₄ alditols (threitol+erythritol). Reaction conditions: xylitol 10 wt%, 135 mL H_2O , 0.5 g 3%Ru- MnO(y%)/C catalyst, 60 bar H_2 , 200°C, 80% xylitol conversion.

The high level of Mn leaching limits the reusability of the MnO-promoted catalyst. After washing the catalyst with water and drying it at 60°C under N_2 , a second run was conducted. A drop in activity (Figure S8), from 220h⁻¹ to 80h⁻¹, was observed. The product distribution was similar but 88% of the Mn remaining at the end of the first run leached during the second run.

Therefore we decided to investigate in more details the nature and the effect of Mn species on the hydrogenolysis of xylitol and more specifically on Mn leaching. The catalytic performances of physical mixtures of Ru/C catalyst with MnO, MnO₂, and a Mn(NO₃)₂ aqueous solution, are summarized in Table 6. All reactions were performed introducing the same amount of Mn species, i.e. 22.5 mg, in the reaction medium, except for Ru/MnO_x. The results are shown in Table 6.

Table 6. Influence of Mn species (22.5 mg Mn) on the performance of the Ru catalyst in the hydrogenolysis reaction of xylitol.

Catalyst	Activity [h ⁻¹]	Carbon selectivity ^[a] [%]					Carbon balance ^[a] [%]		Mn leaching [%]
		Glycols (EG+PG)	GLY	LA	C ₅ alditols	C ₄ alditols	BDO	TOC	

3.1%Ru/MnO(4.5%)/C	220	22	10	traces	19	17	3	84	71	71
2.9%Ru/C + MnO	150	26	13	traces	15	19	-	85	78	64
2.9%Ru/C + MnO₂	170	24	12	traces	15	19	-	85	75	66
2.9%Ru/C + Mn²⁺ ^[b]	160	30	15	traces	10	14	-	81	78	-
2.8%Ru/MnO_x ^[c]	300	27	10	3	7	13	-	72	66	63

Reaction conditions: 10 wt% xylitol; 200°C; 60 bar H₂; 0.5 g catalyst.

^[a] at 80% conversion. ^[b] introduction of 1.71 mL Mn(NO₃)₂ aqueous solution (14.5 g L⁻¹); ^[c] introduction of 0.3 g catalyst (227.5 mg Mn)

The catalytic activities remained in the range of 150-220 h⁻¹ when the different Mn species were introduced with the Ru/C catalyst. The products distributions were also similar and only traces of LA were detected. The epimerization selectivity was higher when Mn was deposited on the support as Mn oxide (19%) than when Mn was added as a physical mixture of Ru/C and MnO or MnO (15%), or as a salt in the aqueous reaction medium (10%). Mn leaching was important in the range of 66% to 71%, regardless of the amount of Mn introduced.

Over the Ru/MnO_x catalyst, the activity was higher (300 h⁻¹), suggesting a better proximity and cooperativity between Ru and Mn. Regarding the products distribution, the selectivities towards glycols and glycerol were similar to the other catalysts, while the selectivity to LA was detectable and attained 3%. No Ru leaching was observed, although the Mn leaching was of 63%.

These results confirm that the association of Mn²⁺ ions with Ru/C may be an efficient catalytic system for the C-C bond cleavage of xylitol into C₂-C₃ products.

The Mn species responsible for the synergy of activity for C-C cleavage may be either MnO on the solid or Mn ions leached into the reaction medium. Over the MnO(4.7%)/C catalyst, leaching of Mn was of only 15% and no conversion of xylitol could be observed, suggesting that the operating conditions were not responsible for the elution. In contrast, over the Ru/MnO/C catalysts, when xylitol was converted, leaching was high suggesting that Ru is required for selective reaction and that Mn leaching was due to the formation of some reaction products. Leaching of MnO has been reported previously under similar conditions.^[28,41] Indeed, in the hydrodeoxygenation of guaiacol in aqueous phase at 160°C under 15 bar H₂ over a Ru-MnO_x/C catalyst, Ishikawa *et al.* attributed the rapid Mn elution during the reaction to the presence of the acidic substrate and intermediates (phenolic compounds).^[41] Recently, Murillo Leo *et al.* similarly explained the high leaching of Ca(OH)₂ used as the support for Ni and Ru catalysts during sorbitol hydrogenolysis to the formation of acidic by-products (as demonstrated by the change of pH at the end of the reaction).^[28]

The comparison of the concentration of LA produced and the amount of Mn leached as a function of time during the reaction over a 3%Ru/MnO(5.6%)/C catalyst (Figure 9) shows some correlation between the two values. The amounts of Mn leached and of LA produced attained a plateau after 5 h and remained constant up to 30 h of reaction. The molar ratio LA/Mn varied in the range 1-1.8. In addition, it was observed that the introduction of the Ru/MnO/C catalyst

in a LA aqueous solution (3.81 mM) at room temperature immediately resulted in the leaching of Mn. These results demonstrate the link between the formation of acidic products and Mn leaching, even at very low concentration of lactate (selectivity < 1%).

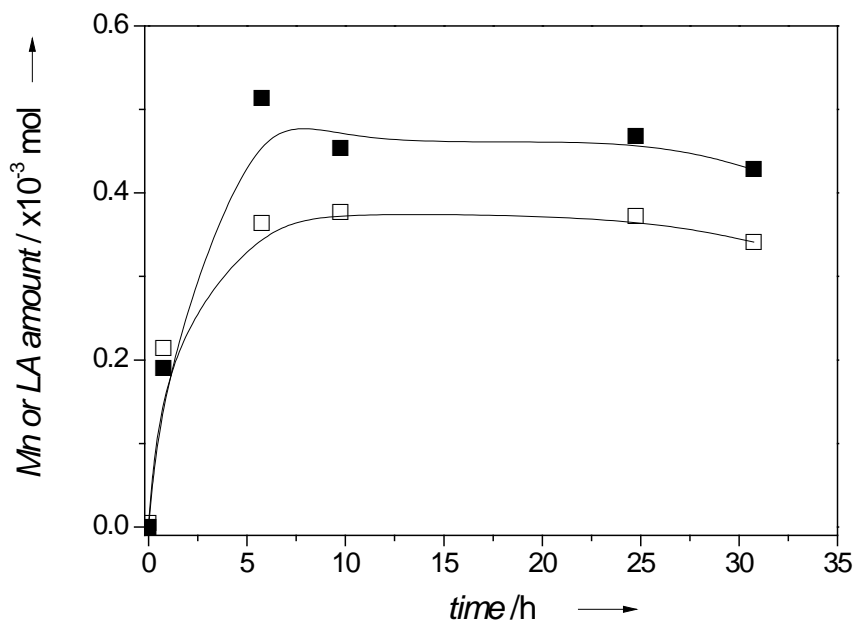


Figure 9. Comparison between leached Mn (□) and produced LA (■) as a function of time for the hydrogenolysis of xylitol over Ru/MnO/C catalyst.

Reaction conditions: xylitol 10 wt%; 135 mL H₂O; 0.5 g 3%Ru/MnO(5.6%)/C catalyst; 60 bar H₂; 200°C.

3. Conclusions

In summary, the addition of a homogeneous base has a strong effect on the xylitol hydrogenolysis mechanism over Ru/C. Without base, fast epimerization and decarbonylation reactions occurred until 80% xylitol conversion. Afterwards, the formed epimers underwent cascade decarbonylation which then produced gaseous light alkanes at full conversion. The addition of Ca(OH)₂ base, even in small quantities, limited these reactions and promoted the retro-aldol reaction. The C₃/C₂ molar ratio of 1.25 is superior to the theoretical value of 1 as EG reacts over Ru catalyst and forms light alkanes such as CH₄. Increasing the amount of base, up to $R_{\text{mol}}(\text{OH}/\text{xylitol}) = 0.68$ improved the selectivity to glycols (EG+PG) but the selectivity to by-product LA (27%) exceeded those to PG and GLY (25% and 24%, respectively). To avoid the production of LA, Ru/MnO/C catalyst, which exhibits the highest amount of basic sites (CO₂-TPD), was the most efficient bifunctional catalyst in absence of base, with high activity (220 h⁻¹) and selectivity to glycols (22%) and glycerol (10%), and only traces of LA. The catalytic response, in term of activity and selectivity towards glycols, improved with the amount of MnO. However, Mn leaching up to 70% was observed, associated with the traces of LA formed even in the absence of added base. The leaching of metal promoter remains a challenge for further works, it is essential to reduce the formation of acidic derivatives.

4. Experimental Section

4.1 Preparation of Catalysts

The monometallic Ru/C catalysts were prepared by wet impregnation using $\text{RuNO}(\text{NO}_3)_3 \cdot x\text{H}_2\text{O}$ (>31.3%, Alpha Aesar). An aqueous solution containing 0.15 g or 0.35 g of Ru in 15 mL of distilled water (for 3wt% Ru/C or 7wt% Ru/C, respectively) was added to a suspension of active carbon (L3S CECA, Table 1, $S_{\text{BET}} = 1095 \text{ m}^2 \cdot \text{g}^{-1}$ and $V_{\text{pores}} = 0.81 \text{ cm}^3 \cdot \text{g}^{-1}$), 5 g in 20 mL water, in a 250 mL round-bottom flask. After stirring for 6h at room temperature, water was removed in a rotary evaporator under 100 mbar at 70°C. The resulting powder was dried at 60°C overnight in an oven under N_2 atmosphere. The solid was reduced under H_2 flow ($100 \text{ mL} \cdot \text{min}^{-1}$) at 450°C for 3 h ($2^\circ\text{C} \cdot \text{min}^{-1}$) and finally passivated under 1% O_2/N_2 gas flow for 30 min at room temperature.

The bifunctional Ru/metal oxide/C (denoted as Ru/ $\text{MO}_x(\text{y})/\text{C}$, where the y in parenthesis represents the measured M wt%) catalysts were prepared by successive wet impregnation. First, the active carbon in suspension in water was impregnated with an aqueous solution of the metallic precursor salt ($[\text{SnCl}_4 \cdot 5\text{H}_2\text{O}]$, 98% Aldrich; $[(\text{NH}_4)_6\text{H}_2\text{W}_{12}\text{O}_{40} \cdot x\text{H}_2\text{O}]$, 99% Fluka; $[\text{Zn}(\text{NO}_3)_2 \cdot 6\text{H}_2\text{O}]$, 99% AppliChem; $[\text{Sr}(\text{NO}_3)_2]$, 99% Fluka; $[\text{Mn}(\text{NO}_3)_2 \cdot 4\text{H}_2\text{O}]$, 98% Merck). After evaporation of water and further drying overnight at 110°C, the solid was calcined at 200°C for 4 h ($2^\circ\text{C} \cdot \text{min}^{-1}$) under air flow ($100 \text{ mL} \cdot \text{min}^{-1}$). Subsequently, the wet impregnation of Ru and the reduction were carried out as described above. The amount of Ru was calculated to obtain a M/Ru mass of approximately 1.5. Ru/MnO/C catalysts containing higher Mn contents were synthesized by increasing the concentration of $\text{Mn}(\text{NO}_3)_2 \cdot 4\text{H}_2\text{O}$ in the aqueous solution.

A Ru/ MnO_x catalyst was prepared by incipient wetness impregnation according to the procedure described elsewhere.^[42] The MnO_x support was first prepared by co-precipitation using 45 mL of 0.5 M $\text{Mn}(\text{NO}_3)_2 \cdot 4\text{H}_2\text{O}$ aqueous solution and 50 mL of 0.5 M Na_2CO_3 (99.95%, Sigma Aldrich) aqueous solution at 80°C (pH 9) for 2 h. After filtration and washing with hot demineralized water, in order to remove any trace of sodium, the solid was dried at 110°C overnight and calcined under air ($100 \text{ mL} \cdot \text{min}^{-1}$) at 500°C for 5 h ($4^\circ\text{C} \cdot \text{min}^{-1}$). Then, an aqueous solution of $\text{RuNO}(\text{NO}_3)_3 \cdot x\text{H}_2\text{O}$ (19 mg of Ru in 1.80 mL) was impregnated on the MnO_x support for 6 h at room temperature. The solid was dried at 110°C overnight and reduced under H_2 flow and passivated as previously.

4.2 Catalyst characterization

The metal loadings of the catalysts were determined after complete dissolution in *aqua regia* at 150°C for 12h and analyzed by inductively coupled plasma optical emission spectroscopy (ICP-OES) analysis (Activa Jobin-Yvon). X-ray diffraction (XRD) patterns were recorded using a Bruker D8A25 diffractometer with $\text{CuK}\alpha$ radiation and multi-channel fast detector LynxEye ($0.04^\circ \cdot \text{s}^{-1}$ over the range $5 \leq 2\theta \leq 80^\circ$). The average crystallite sizes were determined according to the Debye Scherrer equation from the full width at half maximum of the peak with the highest intensity. N_2 physisorption isotherms were obtained at -196°C using a Micrometrics ASAP 2020 sorption analyzer and used for the determination of specific area (BET method) and total pore volume (at $P/P_0 = 0.99$). Prior to the measurement, the sample was degassed under vacuum ($<10^{-4}$ mbar) at 350°C for 7 h ($2^\circ\text{C}\cdot\text{min}^{-1}$). TEM images were taken on a JEOL 2010 instrument operated at 200 keV. Samples were prepared by dispersing the solid in ethanol and then placed onto carbon-coated grids. The average size of Ru particles and their size distribution were determined by measuring ca. 300 particles randomly distributed in the images. Energy dispersive X-ray (EDX) analysis was carried out with an Oxford Link Isis spectrometer. The surface basicity of the catalysts was determined through temperature-programmed desorption of CO_2 (CO_2 -TPD). In a typical run, the reduced sample (about 30 mg) was first pre-treated in He gas ($50 \text{ mL}\cdot\text{min}^{-1}$) at 450°C for 1 h, and then cooled to 100°C. Subsequently, the sample was saturated with 5% v/v CO_2/He ($25 \text{ mL}\cdot\text{min}^{-1}$) at that temperature for 30 min. The TPD profiles were recorded with a thermal conductivity detector (TCD) when heating the sample at $8^\circ\text{C}\cdot\text{min}^{-1}$ from 100°C to 450°C under a continuous flow of He ($50 \text{ mL}\cdot\text{min}^{-1}$).

4.3 Hydrogenolysis reaction

Xylitol hydrogenolysis was performed in a 300 mL Hastelloy Parr autoclave. In a typical experiment, 135 mL of a 10 wt% xylitol (99%, Sigma Aldrich) aqueous solution containing the $\text{Ca}(\text{OH})_2$ base (96%, Merck) and 0.5 g of reduced catalyst were introduced into the reactor. The sealed autoclave was purged three times with 60 bar of Ar to remove the residual air, pressurized with hydrogen, and then heated to 200°C under stirring at 700 rpm. Once the reaction temperature was reached, the pressure was adjusted to 60 bar H_2 and vigorous stirring (1000 rpm) was applied in order to eliminate the diffusion effects. This corresponds to reaction time $t = 0$. During the reaction, liquid samples were periodically collected through a sampling valve; they were filtered over PVDF membranes ($0.45 \mu\text{m}$) before analysis. After reaction, the autoclave was cooled down and the catalyst was separated by vacuum filtration over PVDF membranes ($0.45 \mu\text{m}$).

4.4 Products analysis

Liquid reaction samples were analyzed using two separation methods on two Shimadzu HPLC apparatus. The first one had a Rezex RCM-Monosaccharide Ca^{2+} 8% (700 x 7.80 mm) column

at 60°C, degasified water eluent as the mobile phase (0.4 mL.min⁻¹) and it was connected to a differential refraction detector (Shimadzu RID10A). This one allowed us to separate and quantify the xylitol epimers such as arabitol and adonitol. The second one had a Rezex ROA-Organic Acid H⁺ (300 x 7.80 mm) column at 65°C, degasified sulfuric acid aqueous solution (5 mM) as mobile phase (0.6 mL.min⁻¹), and it was equipped with refractive index diffraction (Shimadzu RID10A) and UV (Shimadzu SPD-M10A) detectors; this one allowed us to separate and quantify the other products such as erythritol, threitol, butanediols, glycerol, ethylene glycol, propylene glycol, lactate, formate, and methanol. Analysis of the products in the gas phase was performed at the end of reaction by collecting the gas phase at room temperature in a gas collecting bag. The gases were analyzed using a μ -GC SRA with MS Agilent 5975 detector. Three columns were set up: alumina plot (10 m x 3 μ m) at 90°C for C₃-C₆ products, Poraplot U (8 m x 30 μ m) for C₂-C₃ products and CO₂, and MolSieve 5A (10 m x 12 μ m) for H₂, CO and CH₄. The total organic carbon (TOC) in solution was measured using a TOC analyzer (Shimadzu TOC-VCHS equipped with ASI-automatic sampler). Comparison of the measured TOC with the TOC calculated from chromatography analysis was used to verify the carbon balance. Based on the initial concentration of xylitol introduced into the reactor, the amount of products transferred from the aqueous phase to the gas phase was calculated by the difference of the TOC value and the measured TOC. The possible metal leaching of the catalyst was detected by ICP-OES of the final liquid mixture. Xylitol conversion (%) was defined as the ratio between the number of xylitol moles consumed in the reaction and the number of xylitol initially loaded. The selectivity to a product (on a carbon basis, %) was reported as the mole fraction of carbon of the product formed and carbon of xylitol consumed. By assuming a pseudo-first order reaction for xylitol consumption over the first three hours, the initial rate coefficient k' (h⁻¹) was obtained for each catalyst and used to calculate the initial reaction activity defined as follows (for simplification, activity is given in h⁻¹), where n_{Ru} is the total number of moles of Ru:

$$\text{Activity} / \text{mol}_{\text{xylitol}} \cdot \text{mol}_{\text{Ru}}^{-1} \cdot \text{h}^{-1} = \frac{k' \times n_{\text{xylitol}}^{\text{initial}}}{n_{\text{Ru}}}$$

Acknowledgments

The financial support was provided by Ecole Doctorale de Chimie Lyon (PhD grant M.R.) and IFP Energies nouvelles. The authors acknowledge the Services Scientifiques of IRCELYON for the characterization of the catalysts.

References

- [1] M. Besson, P. Gallezot, C. Pinel, *Chem. Rev.* **2014**, *114*, 1827–70.
- [2] A. M. Ruppert, K. Weinberg, R. Palkovits, *Angew. Chem. Int. Ed. Engl.* **2012**, *51*, 2564–601.
- [3] George W. Huber, A. Sara Iborra, A. Corma, *Chem. Rev.* **2006**, *106*, 4044–4098.

- [4] G. Petersen, T. Werpy, *Top Value Added Chemicals from Biomass: Results of Screening for Potential Candidates from Sugars and Synthesis Gas, Vol I*, **2004**.
- [5] X. Liu, X. Wang, S. Yao, Y. Jiang, J. Guan, X. Mu, *RSC Adv.* **2014**, *4*, 49501–49520.
- [6] *Final Rep. Eur. Comm. Dir. Energy* **2015**, 183.
- [7] C. M. Osmundsen, K. Egeblad, E. Taarning, in *New Futur. Dev. Catal.* (Ed.: S.L. Suib), Elsevier, **2013**, pp. 73–89.
- [8] H. Yue, Y. Zhao, X. Ma, J. Gong, *Chem. Soc. Rev.* **2012**, *41*, 4218.
- [9] C. A. Staples, J. B. Williams, G. R. Craig, K. M. Roberts, *Chemosphere* **2001**, *43*, 377–383.
- [10] A. Marinas, P. Bruijninx, J. Ftouni, F. J. Urbano, C. Pinel, *Catal. Today* **2015**, *239*, 31–37.
- [11] I. T. Clark, *Ind. Eng. Chem.* **1958**, *50*, 1125–1126.
- [12] D. K. Sohounloue, C. Montassier, J. Barbier, *React. Kinet. Catal. Lett.* **1983**, *22*, 391–397.
- [13] C. Montassier, J. C. Ménézo, L. C. Hoang, C. Renaud, J. Barbier, *J. Mol. Catal.* **1991**, *70*, 99–110.
- [14] L. Zhao, J. H. Zhou, Z. J. Sui, X. G. Zhou, *Chem. Eng. Sci.* **2010**, *65*, 30–35.
- [15] M. Banu, S. Sivasanker, T. M. Sankaranarayanan, P. Venuvanalingam, *Catal. Commun.* **2011**, *12*, 673–677.
- [16] K. L. Deutsch, D. G. Lahr, B. H. Shanks, *Green Chem.* **2012**, *14*, 1635–1642.
- [17] T. Soták, T. Schmidt, M. Hronec, *Appl. Catal. A Gen.* **2013**, *459*, 26–33.
- [18] X. Chen, X. Wang, S. Yao, X. Mu, *Catal. Commun.* **2013**, *39*, 86–89.
- [19] J. Zhang, F. Lu, W. Yu, J. Chen, S. Chen, J. Gao, J. Xu, *Catal. Today* **2014**, *234*, 107–112.
- [20] I. M. Leo, M. L. Granados, J. L. G. Fierro, R. Mariscal, *Chinese J. Catal.* **2014**, *35*, 614–621.
- [21] J. Zhou, G. Liu, Z. Sui, X. Zhou, W. Yuan, *Chinese J. Catal.* **2014**, *35*, 692–702.
- [22] X. Wang, X. Liu, Y. Xu, G. Peng, Q. Cao, X. Mu, *Chinese J. Catal.* **2015**, *36*, 1614–1622.
- [23] W. C. Du, L. P. Zheng, J. J. Shi, S. X. Xia, Z. Y. Hou, *Fuel Process. Technol.* **2015**, *139*, 86–90.
- [24] X. Jin, J. Shen, W. Yan, M. Zhao, P. S. Thapa, B. Subramaniam, R. V. Chaudhari, *ACS Catal.* **2015**, *5*, 6545–6558.
- [25] Y. Jia, H. Liu, *Chinese J. Catal.* **2015**, *36*, 1552–1559.
- [26] R. Vijaya Shanthi, T. M. Sankaranarayanan, R. Mahalakshmy, S. Sivasanker, *J. Environ. Chem. Eng.* **2015**, *3*, 1752–1757.
- [27] J. Zhang, F. Lu, W. Yu, R. Lu, J. Xu, *Chinese J. Catal.* **2016**, *37*, 177–183.
- [28] I. Murillo Leo, M. López Granados, J. L. G. Fierro, R. Mariscal, *Appl. Catal. B Environ.* **2016**, *185*, 141–149.
- [29] Y. Jia, H. Liu, *Catal. Sci. Technol.* **2016**, *6*, 7042–7052.
- [30] L. Ye, X. Duan, H. Lin, Y. Yuan, *Catal. Today* **2012**, *183*, 65–71.

- [31] X. Jin, B. Subramaniam, R. V. Chaudhari, *Novel Materials for Catalysis and Fuels Processing*, American Chemical Society, Washington, DC, **2013**.
- [32] A. H. Zacher, J. G. Frye Jr., T. A. Werpy, D. J. Miller, *Chem. Ind.* **2005**, *104*, 165–173.
- [33] F. Auneau, M. Berchu, G. Aubert, C. Pinel, M. Besson, D. Todaro, M. Bernardi, T. Ponsetti, R. Di Felice, *Catal. Today* **2014**, *234*, 100–106.
- [34] H. Liu, Z. Huang, C. Xia, Y. Jia, J. Chen, H. Liu, *ChemCatChem* **2014**, *6*, 2918–2928.
- [35] J. Sun, H. Liu, *Catal. Today* **2014**, *234*, 75–82.
- [36] Z. Huang, J. Chen, Y. Jia, H. Liu, C. Xia, H. Liu, *Appl. Catal. B Environ.* **2014**, *147*, 377–386.
- [37] J. Sun, H. Liu, *Green Chem.* **2011**, *13*, 135.
- [38] X. Wang, F. Wu, S. Yao, Y. Jiang, J. Guan, X. Mu, *Chem. Lett.* **2012**, *41*, 476–478.
- [39] Z. Zhou, X. Li, T. Zeng, W. Hong, Z. Cheng, W. Yuan, *Chinese J. Chem. Eng.* **2010**, *18*, 384–390.
- [40] T. Deng, H. Liu, *J. Mol. Catal. A Chem.* **2014**, *388–389*, 66–73.
- [41] M. Ishikawa, M. Tamura, Y. Nakagawa, K. Tomishige, *Appl. Catal. B Environ.* **2016**, *182*, 193–203.
- [42] B. Zhang, Y. Zhu, G. Ding, H. Zheng, Y. Li, *Green Chem.* **2012**, *14*, 3402.
- [43] K. S. W. Sing, D. H. Everett, R. A. W. Haul, L. Moscou, Pierotti R. A., Rouquérol J., Siemieniewska T., *Pure Appl. Chem.* **1985**, *57*, 603–619.
- [44] J. Liu, P. Bai, X. S. Zhao, *Phys. Chem. Chem. Phys.* **2011**, *13*, 3758–63.
- [45] J. Jae, G. A. Tompsett, A. J. Foster, K. D. Hammond, S. M. Auerbach, R. F. Lobo, G. W. Huber, *J. Catal.* **2011**, *279*, 257–268.
- [46] S. Wang, K. Yin, Y. Zhang, H. Liu, *ACS Catal.* **2013**, *3*, 2112–2121.
- [47] T. Deng, H. Liu, *Green Chem.* **2013**, *15*, 116–124.
- [48] S. G. Wettstein, J. Q. Bond, D. M. Alonso, H. N. Pham, A. K. Datye, J. A. Dumesic, *Appl. Catal. B Environ.* **2012**, *117–118*, 321–329.
- [49] M. A. Alvarez-Merino, F. Carrasco-Marín, J. L. G. Fierro, C. Moreno-Castilla, *J. Catal.* **2000**, *192*, 363–373.
- [50] E. I. Ross-Medgaarden, I. E. Wachs, *J. Phys. Chem. C* **2007**, *111*, 15089–15099.
- [51] K. Tajvidi, P. J. C. Hausoul, R. Palkovits, *ChemSusChem* **2014**, *7*, 1311–7.
- [52] P. J. C. Hausoul, L. Negahdar, K. Schute, R. Palkovits, *ChemSusChem* **2015**, *9*, 3323–3330.
- [53] P. J. C. Hausoul, A. K. Beine, L. Neghadar, R. Palkovits, *Catal. Sci. Technol.* **2017**, *7*, 56–63.
- [54] F. van der Klis, L. Gootjes, J. van Haveren, D. S. van Es, J. H. Bitter, *Green Chem.* **2015**, *17*, 3900–3909.
- [55] R. Ooms, M. Dusselier, J. A. Geboers, B. Op de Beeck, R. Verhaeven, E. Gobechiya, J. A. Martens, A. Redl, B. F. Sels, *Green Chem.* **2014**, *16*, 695.
- [56] K. Wang, M. C. Hawley, T. D. Furney, *Ind. Eng. Chem. Res.* **1995**, *34*, 3766–3770.
- [57] J. W. Shabaker, R. R. Davda, G. W. Huber, R. D. Cortright, J. A. Dumesic, *J. Catal.* **2003**, *215*, 344–352.

- [58] A. C. B. Silva, A. P. G. de Sousa, J. D. Ardisson, H. G. L. Siebald, E. Moura, E. N. dos Santos, N. D. S. Mohallem, R. M. Lago, *Mater. Res.* **2003**, *6*, 137–144.
- [59] D. L. Hoang, S. A.-F. Farrage, J. Radnik, M.-M. Pohl, M. Schneider, H. Lieske, A. Martin, *Appl. Catal. A Gen.* **2007**, *333*, 67–77.
- [60] C. Liu, C. Zhang, S. Sun, K. Liu, S. Hao, J. Xu, Y. Zhu, Y. Li, *ACS Catal.* **2015**, *5*, 4612–4623.